Progress in Organic Coatings 160 (2021) 106527

Contents lists available at ScienceDirect

Progress in Organic Coatings

journal homepage: www.elsevier.com/locate/porgcoat

# Emerging waste-free non-destructive system based on molecular sensors originating from novel europium complexes for in-situ determination of polymer coating thickness

Monika Topa [a], Anna Chachaj-Brekiesz [b], Tomasz Świergosz [c], Roman Popielarz [a], Joanna Ortyl [a,d,*]

[a] Department of Biotechnology and Physical Chemistry, Faculty of Chemical Engineering and Technology, Cracow University of Technology, Warszawska 24, 30-155 Kraków, Poland
[b] Department of General Chemistry, Faculty of Chemistry, Jagiellonian University, Gronostajowa 2, 30-387 Kraków, Poland
[c] Department of Chemical Technology and Environmental Analysis, Faculty of Chemical Engineering and Technology, Cracow University of Technology, Warszawska 24, 31-155 Kraków, Poland
[d] Photo HiTech Ltd., Life Science Park, Bobrzyńskiego 14, 30-348 Kraków, Poland

ARTICLE INFO

*Keywords:*
Cationic photopolymerisation
Europium complexes
Fluorescence Probe Technology
Free radical photopolymerisation
Luminescence spectroscopy
Reaction monitoring

ABSTRACT

Herein, novel europium(III) complex derivatives dedicated to polymer chemistry applications as molecular sensors have been reported. The following are among them tris(4,4,4-trifluoro-1-phenylbutane-1,3-dione) europium(III) (BTA) and tris(4,4,4-trifluoro-1-(2-naphthyl)butane-1,3-dione)europium(III)] (NTA). To obtain the relevant europium complexes, they were coordinated with the corresponding ligands, e.g., 4-phenyl-2,6-bis (2-pyridyl)pyridine (PPP), 2,2′-bipyridine (Bpy), 2-(2-pyridyl)-1,3-benzothiazole (PBT) and 2-(2-pyridyl)imidazo [1,2-*a*]pyridine (PIP). The application of these compounds as luminescent sensors to monitor the kinetics of cationic photopolymerisation of monomers has been investigated along with the determination of optical properties. Ultimately, the possibility of employing europium(III) complexes as thickness sensors for polymer coatings resulting from the free radical photopolymerisation of trimethylolpropane triacrylate was measured using Fluorescence Probe Technology developing a zero-waste, non-destructive method for in-situ determination of polymer coating thickness.

## 1. Introduction

Monitoring the thickness of polymer coatings to control the properties of the final product remains a high priority concern for industry [1]. In this context, several parameters have an impact on polymer thickness, including viscosity, temperature, and web speed [2,3]. Therefore, some unintended variations may occur in coating operations [4–7]. Moreover, a coating that is too thin will not be resistant to decomposition, and the surface of any such coating will suffer rapid corrosion if applied to a metal object [8]. In addition, an over-thin coating results in insufficient covering strength and protective capabilities, requiring additional time to recoat the surface [9]. On the other hand, coating that is too thick increases the cost of materials and the final product itself, rather than necessarily guaranteeing added resistance or visual qualities [10,11]. Thus, an overly thick coating can result in cracking, peeling or enhanced drying/curing time [12].

Wet film thickness (WFT) measurement involves measuring the shape of the surface and the expected wet film thickness range. Another type of coating thickness measurement is dry film thickness (DFT) [13]. For this purpose, verification of dry film thickness is possible in a non-destructive or destructive way, e.g., in the case of multilayer coatings. Designed for the measurement of dry film thickness non-destructive methods are mainly implemented as (i) the magnetic method - for measurements of non-magnetic coatings applied on a magnetic background - the method consists in measuring the force necessary to detach a permanent magnet or electromagnet from the surface covered with the coating under examination, or in measuring the force with an effect by which the magnet is attracted by the magnetic background through the

* Corresponding author at: Department of Biotechnology and Physical Chemistry, Faculty of Chemical Engineering and Technology, Cracow University of Technology, Warszawska 24, 30-155 Kraków, Poland.
*E-mail address:* jortyl@pk.edu.pl (J. Ortyl).

https://doi.org/10.1016/j.porgcoat.2021.106527
Received 24 May 2021; Received in revised form 22 July 2021; Accepted 12 September 2021
Available online 21 September 2021

coating; (ii) the electromagnetic method - applied to measurements of non-magnetic coatings applied on a magnetic substrate - the method consists in measuring changes of sensor inductance; (iii) the eddy current testing, used to measure the thickness of insulating coatings on a non-magnetic metal substrate, non-magnetic metal coatings on a non-metallic substrate, or, non-magnetic metal coatings on a non-magnetic metal substrate; and (iv) the radiometric (β-reflectance) method used to measure the thickness of coatings made only of materials of known chemical composition - this method relies on the use of differences in β-reflectance intensity of different materials. Moreover, methods (i) up to (iii) require the usage of electronic meters that measure the thickness of insulating coatings on non-magnetic metal substrates (NFe - for example, aluminium, copper, brass, stainless steel, bronze, magnesium, zinc) and non-magnetic coatings on iron or steel (Fe) substrates. Furthermore, the operation of gauges used to measure dry film thickness in non-destructive methods is based on two principles: (1) the measurement of magnetic induction for layer measurements thru iron or steel (Fe-type) substrates, or principle (2) whereby eddy current measurements are conducted on metal substrates that do not exhibit magnetic properties (NFe-type) [14,15].

Alternatively, another type of dry coating thickness measurement involves destructive measurements covering mechanical, chemical, and electrochemical methods. Mechanical methods (including microscopic) involve the observation of a cross section of the coating using, for example, a scanning electron microscope. Chemical methods include, but are not limited to, a complete chemical dissolution of the coating without disturbing the metal substrate, or a droplet method comprising local dissolution of the coating by successive portions of solvent droplets, or a stream method comprising chemical dissolution of the coating by a stream of solution. The electrochemical (coulometric) method is also classified as destructive and involves anodic dissolution of the coating on a well-defined surface. However, all the above-mentioned destructive methods require interaction with the applied coating and cause permanent local damage, therefore they cannot be used for testing on the final elements of the product, but can only be used on samples specially selected for this purpose [14,15].

Providing an alternative to both WFT - Wet Film Thickness and DFT - Dry Film Thickness testing methods described above, luminescence spectroscopy and luminescent chemical sensors can be employed. Therefore, a number of fluorescent molecular sensors have been developed until now [16–19]. Many sensors were used to monitor the kinetics of photopolymerisation processes using Fluorescence Probe Technology (FPT) [20–24]. Measurement luminescence intensity at any wavelength under certain measurement conditions is proportional to the sensor concentration and to the film thickness. However, when the chemosensor concentration is held constant, the measured fluorescence intensity is only proportional to the film thickness. It has been shown that even when coatings are applied to substrates that are also fluorescent, and sometimes with an intensity that far exceeds the intensity of the fluorescence coming from the sensor in the coating, it is still possible to monitor changes in coating thickness with this method [21,25–28]. A luminescence phenomenon, occurring in organic compounds of complex metals and especially rare earth elements (block f), has been the subject of research in various fields of science, ranging from medicine [29–32], biochemistry [16], followed by new materials such as molecular devices for UV–Vis, UV-NIR light conversion [33] and for OLEDs production [34,35]. These compounds have also a number of unique luminescent properties [35–42]. The emission spectra of such coordination compounds are characterized by a long lifetime of the excited state (about $10^{-3}$ s) [43,44], while for average organic chromophores it is on average $10^{-8}$ s. In addition, rare earth complex compounds have a large Stokes shift [45–47] and their emission spectra are very narrow and intense [48–54].

Furthermore, rare earth complexes are used in time-resolved delayed luminescence imaging microscopy (TR-DLIM) [55], as biomarkers (so-called lanthanide luminescent bioprobes - LLBs) [56] in medicine for cell imaging [57], cancer tissue detection [58], as well as in drug delivery monitoring systems [59] and analysis of key biochemical metabolites [60]. Moreover, lanthanide compounds are utilized during magnetic resonance imaging (MRI), in which gadolinium complex is used as a contrast agent [61–63]. Thereby, all this allows the synthesis of non-toxic luminescent chemical sensors that are safe for the human body through the proper selection of organic ligands and metal as the coordination centre. All this has led scientists from around the world to design novel lanthanide complexes. There has been an especially significant effort to develop europium complexes as sensors because of their intense luminescence and good solubility [48–51,61–64].

Herein, we report new organic-inorganic europium(III) complexes that have the potential to find applications in polymer chemistry as chemical molecular sensors for monitoring and quality control of photopolymerisation processes. Several spectroscopic measurements were carried out to determine parameters such as Stokes shift, molar extinction coefficient, and monochromaticity. The suitability of these compounds as luminescent sensors to monitor the kinetics of cationic photopolymerisation processes of TEGDVE monomer was investigated. Finally, the usefulness of europium(III) complexes as thickness sensors for polymer coatings obtained by free-radical photopolymerisation was measured using the FPT technique.

## 2. Experimental

### 2.1. Materials

All chemicals and solvents employed in this investigation were at least of reagent grade and were used as received. In this work, eight of trivalent europium complexes were studied in the role of luminescent molecular probes for monitoring the cationic photopolymerisation and control the thickness of polymer coatings. There were derivatives of tris (4,4,4-trifluoro-1-phenylbutane-1,3-dione)europium(III) (BTA) and tris (4,4,4-trifluoro-1-(2-naphthyl)butane-1,3-dione)europium(III)] (NTA). To obtain the europium complexes, they were coordinated with appropriate ligands, such as: 4-phenyl-2,6-bis(2-pyridyl)pyridine (PPP), 2,2′-bipyridine (Bpy), 2-(2-pyridyl)-1,3-benzothiazole (PBT) and 2-(2-pyridyl)imidazo[1,2-*a*]pyridine (PIP). Structures and acronyms of the europium(III) complexes are shown in Fig. 1. The general synthesis procedures for obtaining the complexes are described in the Electronic Supplementary Information (ESI).

In addition, triethylene glycol divinyl ether (TEGDVE, Sigma Aldrich) as a model vinyl monomer and diphenyliodonium hexafluorophosphate (HIP, Alfa Aesar) as a cationic photoinitiator for the cationic photopolymerisation process were employed. On the other hand, trimethylolpropane triacrylate (TMPTA, Sigma Aldrich) and 2,2-dimethoxy-2-phenylacetophenone (OMEGA, Sigma Aldrich) were utilized for a radical photopolymerisation as acrylate monomer and a free radical photoinitiator, respectively. In order to explain the decrease in the intensity of the luminescence of the studied europium (III) complexes, polyethylene glycol diacrylate (PEGDA 200, Sigma Aldrich) was used. The chemical structure of the monomers and photoinitiators are presented in Fig. 2.

### 2.2. Spectral measurements

The absorption and luminescence spectra of europium(III) complexes were measured in acetonitrile (Sigma Aldrich), using the Silver-Nova spectrometer (StellarNet, Inc., USA), in combination with a broadband tungsten-deuterium UV–Vis light source (StellarNet, Inc., USA) and a quartz cuvette with 1.0 cm optical path. Following, the absorbance data were converted into extinction coefficients. All measurements were conducted at ambient temperature (25 °C) in a quartz cuvette (path length 10 mm × 10 mm) in the right-angle configuration. The optical fiber applied to the transmission of light between the measurement point and the spectrometer was manufactured from PMMA

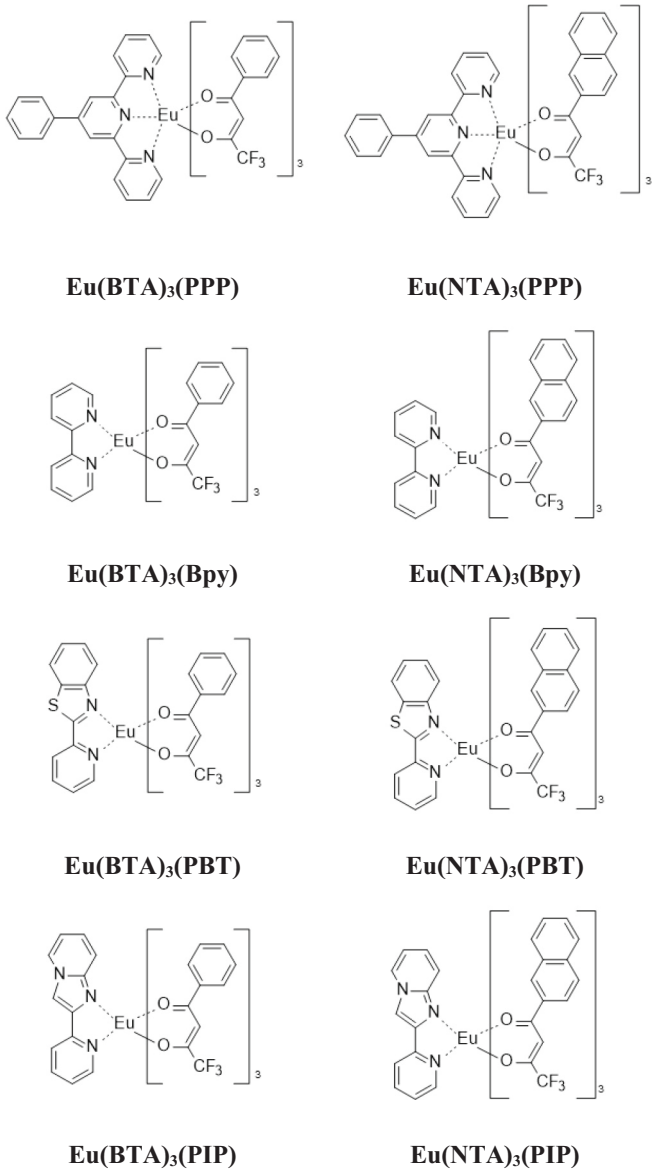


**Fig. 1.** Structures of the europium(III) complexes.

fiber with a 2 mm core (Fibrochem, Poland).

### 2.3. Photoluminescence quantum yields for europium(III) complexes

Photoluminescence quantum yield (PQY) determinations (using the spectrofluorometer FluoroMAX 4Plus from Horiba, Kyoto, Japan) were conducted using a comparative method using quinine sulphate in 0.5 mol/L $H_2SO_4$ (fluorescence max 456 nm, useful excitation range 275–400 (max 350) nm, absolute PQY = 0.546 in 0.5 mol/L $H_2SO_4$) as a standard (Figs. S17–18) [65]. All solutions were prepared in absorption range 0.05–0.1 (310 nm) in order to eliminate concentration quenching effects and L-42 optical filter (340–420 nm) was employed. The samples were excited at 310 nm and the luminescence spectra were acquired between 350 and 750 nm. The PQY was calculated as:

$$\Phi = \Phi_{st}\frac{n^2\left(1-10^{-A_{st}}\right)\int I_{em}dv}{n_{st}^2\left(1-10^{-A}\right)\int I_{em}^{st}dv}$$

where:

$\Phi$ and $\Phi_{st}$ – the quantum yield of a sample and the standard
$A$ and $A_{st}$ – absorption of a sample and the standard at 310 nm
$\int I_{em}dv$ and $\int I_{em}{}^{st}dv$ – integral of fluorescence intensity of a sample and the standard
$n$ and $n_{st}$ – the refractive index of solvent used for a sample and the standard.

### 2.4. Sample preparation

Samples for the Fluorescence Probe Technology (FPT) photopolymerisation studies were prepared in dark amber glass vials in a dark room by dissolving the photoinitiator: diphenyliodonium hexafluorophosphate (HIP) or 2,2-dimethoxy-2-phenylacetophenone (OMEGA) and each europium(III) complexes in the monomer according to the following proportions in order to obtain the concentration of 1.0% by weight photoinitiator and 0.1% by weight europium(III) complexes. Prepared samples in glass vials containing the composition were individually wrapped in aluminium foil and stored in a dark storage area to protect from incidental exposure to daylight. Before measurement, two drops of the composition were placed in the middle of a microscope slide (75 mm × 25 mm × 1 mm), equipped with two 0.09 mm thick spacers located on the slide sides. Then, the slide was covered with another microscope slide to form a sandwich structure. These slides were compressed with clips over both slides. Afterwards, it was placed in the measurement chamber. Prior to measurement, the sample was thermostated for five minutes at 25 °C. Necessary microscope slides of 26 mm × 76 mm × 1 mm from Menzel-Glaser were used to prepare thin film samples according to ISO 8037/I. Moreover, multiple spacers of adhesive paper were used and finally, the thickness of the samples was measured using an electronic micrometre.

### 2.5. Monitoring luminescence changes

The FPT apparatus consisted of a sample chamber equipped with a SilverNova miniature CCD spectrometer (StellarNet, Inc., USA) connected to a microcomputer for data acquisition and UV-LED emitting wavelengths of $\lambda_{max}$ = 320 nm (UVTOP315-BL-TO39, Roithner LaserTechnik GmbH, Austria) incorporated in the sensor head. All FPT photopolymerisation reaction experiments were conducted under controlled thermostatic conditions.

For this purpose, a specially designed measuring chamber, impervious to daylight, was equipped with a high accuracy (±0.1 °C) thermostatic head. An electronically controlled Peltier cell was used as a heat pump to maintain the set temperature inside the chamber. Depending on the temperature difference between the inside of the chamber and the environment, the cell transfers heat either outside or inside the chamber. The measuring head, chamber base, and thermostatic head were constructed from aluminium, while the walls were composed of a piece of 4-inch stainless steel tubing with an outer diameter of 101.6 mm and a wall thickness of 2 mm. Besides, Teflon was used as a heat insulator inside the chamber and a diode sensing head was attached to the base of the chamber. The composition sample was directly adjacent to the diode. UV light from the LED illuminated an approximately 5 mm spot within the thin film sample. The light from the spot was transmitted to the spectrometer via a 2 mm diameter PMMA optical fiber. The UV LED was supplied with a constant current of 23 mA (~1 mW) from a suitable stabilized DC source. The free radical and cationic photopolymerisation processes were conducted at an ambient temperature of 25 °C using an ITC4020 thermostat (Thorlabs Inc., USA). The instrumentation of the measurement system mentioned above has already been published previously [66].

### 2.6. Monitoring the photopolymerisation processes by real-time FT-IR

The cationic and radical photopolymerisation was investigated using the real-time FT-IR method along with FT-IR i10 NICOLET™ spec-

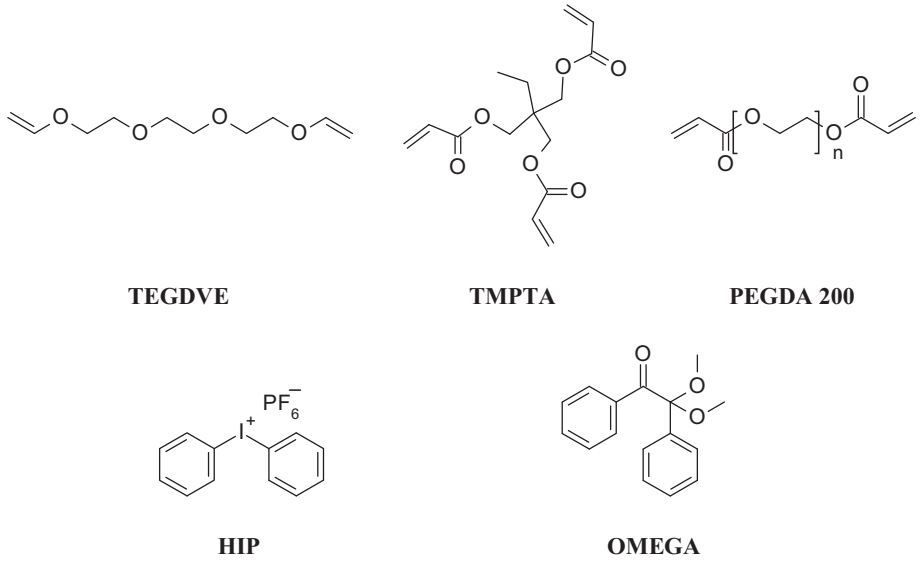


**Fig. 2.** Chemical structures of the monomers and photoinitiators.

trometer with a horizontal adapter (from Thermo Scientific, Waltham, MA, USA). The compositions for photopolymerisation measurements were prepared by dissolution of [4-phenyl-2,6-bis(2-pyridyl)pyridine) tris(4,4,4-trifluoro-1-phenylbutane-1,3-dione)europium(III)] (Eu(BTA)$_3$(PPP) (0.1% w/w)/diphenyliodonium hexafluorophosphate (HIP, Alfa Aesar) (1% w/w) in the TEGDVE and TMPTA monomers. All compositions were prepared in dark glass vials and stored in dark until utilization. Because the decrease of absorption of the peak area is directly proportional to the number of polymerized groups, the degree of conversion of the function group was calculated by measuring the peak area at each time of the reaction by using Eq. (1)

$$C_{FT-IR}\,[\%] = \left(1 - \frac{A_{After}}{A_{Before}}\right) * 100\% \quad (1)$$

where: $A_{Before}$ - is an area of the absorbance peak characteristic for used monomer and type of photopolymerisation before polymerisation process, and $A_{After}$ - is an area of the same absorbance peak, but after polymerisation process.

The experiments were carried out in laminate, the formulations (25 μm thick) were sandwiched between two polypropylene films to reduce the oxygen inhibition. The values of the characteristic absorbance peak for studied monomers were given below for each type of photopolymerisation. The evaluation of vinyl group content was continuously followed at about 1634 cm$^{-1}$ for 900 s (Fig. S45), acrylate group content was continuously followed at about 1634 cm$^{-1}$ for 900 s (Fig. S46). The light source for the real-time FT-IR method for the polymerisation of TEGDVE and TMPTA monomers was a diode from Thorlabs Inc., Tampa, FL, USA (350 mA, 0.5 mW/cm$^2$). The UV-LED was started 10 s after the start of spectral registration. The distance between the irradiation source and formulation is 2.1 cm.

## 3. Results and discussion

### 3.1. Spectroscopic properties of europium(III) complexes

According to the first step of the conducted experiments, the absorption and emission characteristics of europium(III) complexes in acetonitrile were investigated. The absorption spectra of the analysed compounds are presented in Fig. 3, showing that in acetonitrile the europium(III) complexes have absorption characteristics in the UV range up to 400 nm. Differences in the structure of the europium(III)-coordinated ligands are responsible for the varying absorption

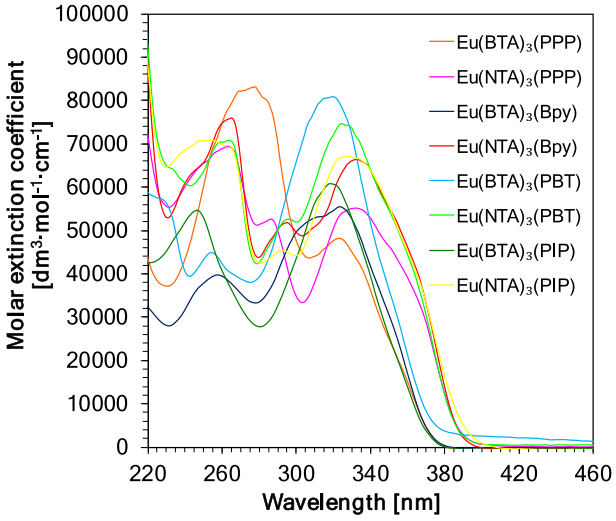


**Fig. 3.** UV–visible absorption spectra of the europium(III) complexes in acetonitrile.

maxima. To demonstrate the exact characterization, the obtained spectral data are summarized in Table 1. From the acquired results, it was observed that the europium(III) complexes exhibit two absorbance bands; one short-wave band found in the range of 200–300 nm, and the other long-wave band found in the range of 300–400 nm.

Fig. 4 illustrates the absorption spectra of europium(III) complexes containing the same diketone (4,4,4-trifluoro-1-phenylbutane-1,3-dione (BTA) in Fig. 4(A) and 4,4,4-trifluoro-1- (2-naphthyl)butane-1,3-dione (NTA) in Fig. 4(B) together with different stabilizing ligands. Then, it was observed that the type of stabilizing ligand does not affect the shift value of the absorption spectrum, but only its intensity. The highest absorbance values are achieved by europium(III) complexes conjugated with the stabilizing ligand PBT (Eu(BTA)$_3$PBT and Eu(NTA)$_3$PBT). It is about 80,000 [dm$^3$ mol$^{-1}$ cm$^{-1}$]. On the other hand, the lowest absorbance values are reached by europium(III) complexes conjugated with the stabilizing ligand PPP (Eu(BTA)$_3$PPP and Eu(NTA)$_3$PPP).

Furthermore, Fig. 5 shows the changes in absorbance properties due to the change of diketone in the structure of europium(III) complexes,

**Table 1**
Spectral characteristics of the europium(III) complexes.

| Compound symbol | Absorption characteristics | | Emission characteristics at 320 nm excitation and 50 s integration time | | | | | Emission characteristics at 365 nm excitation and 400 s integration time | | | | | Stokes shift $\Delta\bar{\nu}$ [$cm^{-1}$] | Quantum yield Φ [%] |
|---|---|---|---|---|---|---|---|---|---|---|---|---|---|---|
| | | | $^5D_0$-$^7F_2$ | | $^5D_0$-$^7F_1$ | | Monohr. | $^5D_0$-$^7F_2$ | | $^5D_0$-$^7F_1$ | | Monohr. | | |
| | $\lambda_{max\text{-}ab}$ [nm] | $\varepsilon_{max}$ [$dm^3 \cdot mol^{-1} \cdot cm^{-1}$] | $I_{max\text{-}lum}$ [rel.u.] | $\lambda_{max\text{-}lum}$ [nm] | $I_{max\text{-}lum}$ [rel.u.] | $\lambda_{max\text{-}lum}$ [nm] | | $I_{max\text{-}lum}$ [rel.u.] | $\lambda_{max\text{-}lum}$ [nm] | $I_{max\text{-}lum}$ [rel.u.] | $\lambda_{max\text{-}lum}$ [nm] | | | |
| Eu(BTA)$_3$(PPP) | 323.3 | 48,185 | 1720 | 614.9 | 128 | 592.8 | 13.46 | 981 | 615.8 | 105 | 593.4 | 9.30 | 13,868 | 15.0 |
| Eu(NTA)$_3$(PPP) | 331.6 | 55,164 | 2924 | 613.9 | 181 | 592.4 | 16.18 | 686 | 614.0 | 74 | 593.8 | 9.25 | 14,667 | 27.4 |
| Eu(BTA)$_3$(Bpy) | 323.6 | 55,451 | 1747 | 612.7 | 108 | 591.8 | 16.19 | 1179 | 612.7 | 102 | 592.1 | 11.59 | 14,580 | 13.4 |
| Eu(NTA)$_3$(Bpy) | 332.7 | 66,333 | 2884 | 612.7 | 153 | 592.8 | 18.88 | 3471 | 612.7 | 221 | 592.4 | 15.71 | 13,735 | 45.9 |
| Eu(BTA)$_3$(PBT) | 320.2 | 80,840 | 97 | 592.8 | 40 | 592.4 | 2.43 | 653 | 612.7 | 66 | 592.8 | 9.93 | 14,360 | 33.6 |
| Eu(NTA)$_3$(PBT) | 324.4 | 74,632 | 1965 | 612.7 | 97 | 592.8 | 20.21 | 3498 | 612.7 | 196 | 593.1 | 17.80 | 14,504 | 33.6 |
| Eu(BTA)3(PIP) | 318.3 | 60,794 | 2523 | 612.7 | 168 | 592.8 | 14.99 | 1686 | 612.7 | 137 | 591.8 | 12.30 | 15,095 | 57.6 |
| Eu(NTA)$_3$(PIP) | 327.0 | 67,150 | 1631 | 612.7 | 85 | 592.8 | 19.24 | 2164 | 612.7 | 144 | 592.8 | 15.03 | 14,259 | 67.4 |

$\lambda_{max\text{-}ab}$ – position of absorption maximum for the long-wave band [nm].
$\varepsilon_{max}$ – molar extinction coefficient measured at $\lambda_{max\text{-}ab}$ [$dm^3 \cdot mol^{-1} \cdot cm^{-1}$].
$\lambda_{max\text{-}lum}$ – position of maximum luminescence intensity [nm].
$I_{max\text{-}lum}$ – intensity at $\lambda_{max\text{-}lum}$ [a.u.]
$\Delta\bar{\nu}$ – Stokes shift (i.e., the difference between the positions of the absorption and emission band maxima) [$cm^{-1}$].
Φ – Photoluminescence quantum yields [%].

represented by (4,4,4-trifluoro-1-phenylbutane-1,3-dione) and 4,4,4-trifluoro-1-(2-naphthyl) butane-1,3-dione, respectively. The bathochrome effect can be observed for all complex compounds coordinated by (2-naphthyl)butane-1,3-dione diketone - NTA upon analysis of these data.

In conclusion, the type of stabilizing ligand in the structure of the complex does not contribute to the shift of the absorption spectrum, but only to the intensity. On the other hand, the type of diketone in the structure of europium(III) complexes affects the value of the absorption spectrum shift, and to a small extent the intensity.

Moreover, the luminescence characteristics of the europium(III) complexes were analysed at two different excitation wavelengths: $\lambda_{max}$ = 320 nm and $\lambda_{max}$ = 365 nm. The following Fig. 6 shows that the structure of the analysed europium(III) complexes has an extremely significant effect on the luminescence intensity. Each of the obtained complexes exhibits europium(III) characteristic red luminescence upon irradiation with a UV lamp of maximum wavelength 320 nm. Besides, the europium(III) complexes have narrow emission peaks characteristic for rare earth complexes. The luminescence intensity of these complexes strongly depends on the type of diketone ligand and the stabilizing ligand implemented into the structure of the complexes.

The emission of europium(III) complexes comes from electronic transitions within the f shell (4f → 4f). The efficiency of Eu(III) ion emission in these compounds depends on the efficiency of LMCT transition (ligand-metal charge transition), as well as on the electron-donor-acceptor properties of the substituents in the structure of ligands coordinated with the central metal. Emission peaks that occur at wavelengths: 580 nm, 592 nm, 612 nm, 652 nm, 703 nm correspond to electronic f-f transitions. These transitions are: $^5D_0$-$^7F_0$ (usually highly prohibited), $^5D_0 \Rightarrow {}^7F_1$, $^5D_0 \Rightarrow {}^7F_2$, $^5D_0 \Rightarrow {}^7F_3$, $^5D_0 \Rightarrow {}^7F_4$, $^5D_0 \Rightarrow {}^7F_0$, $^5D_0 \Rightarrow {}^7F_0$. Of these, the dominant emission occurs at the dipole transition ($^5D_0 \Rightarrow {}^7F_2$) at 612 nm. Nevertheless, the type of built-in diketone substituents affects the value of luminescence intensity: in each case, the europium (III) complexes coordinated with the BTA diketone generally have a higher luminescence intensity than the europium complexes coordinated with the NTA diketone and the same stabilizing ligand (Figs. S9–S16). In addition, the PPP stabilizing ligand in the structure of the europium(III) complexes has a slight effect on the shift of the emission spectrum towards longer wavelengths (Fig. 7).

Another important luminescent property of the lanthanide complex is the quantum yield, defined as the ratio of the number of emitted photons to the number of photons absorbed during the excitation of the sample. The quantum yield of the studied europium(III) complexes was calculated against the standard. In the relative method, the quantum yield of the unknown europium complex is compared with that of the reference sample, which is selected so that its photophysical properties resemble those of the sample. To determine the quantum yield of the luminescence of the studied europium(III) complexes, quinine sulphate in 0.5 mol/L $H_2SO_4$ as a standard was used [65]. The standard must emit in the same spectral region as the lanthanide ion. Most of the reference materials are organic compounds which show broadband emission, while the lanthanide ions show line-like emission. The calculated values of relative quantum yield ranged from 13.4% for [(2,2′-bipyridine)tris (4,4,4-trifluoro-1-phenyl)butane-1,3-dione)europium(III)] (Eu (BTA)$_3$(Bpy)) to as much as 64.7% for [(2-(2-pyridyl)imidazo[1,2-*a*] pyridine)tris(4,4,4-trifluoro-1-(2-naphthyl)butane-1,3-dione)europium (III)], (Eu(NTA)$_3$(PIP)). Interestingly, the europium complexes coordinated with tris (4,4,4-trifluoro-1- (2-naphthyl) butane-1,3-dione) europium (III)] (NTA) generally have correspondingly higher quantum yields than complexes coordinated with the same ligands having the tris (4,4,4-trifluoro-1-phenylbutane-1,3-dione) europium (III) (BTA) substituent. The different quantum yield of the obtained europium(III) complexes confirms the different intensity of the luminescence of these complexes.

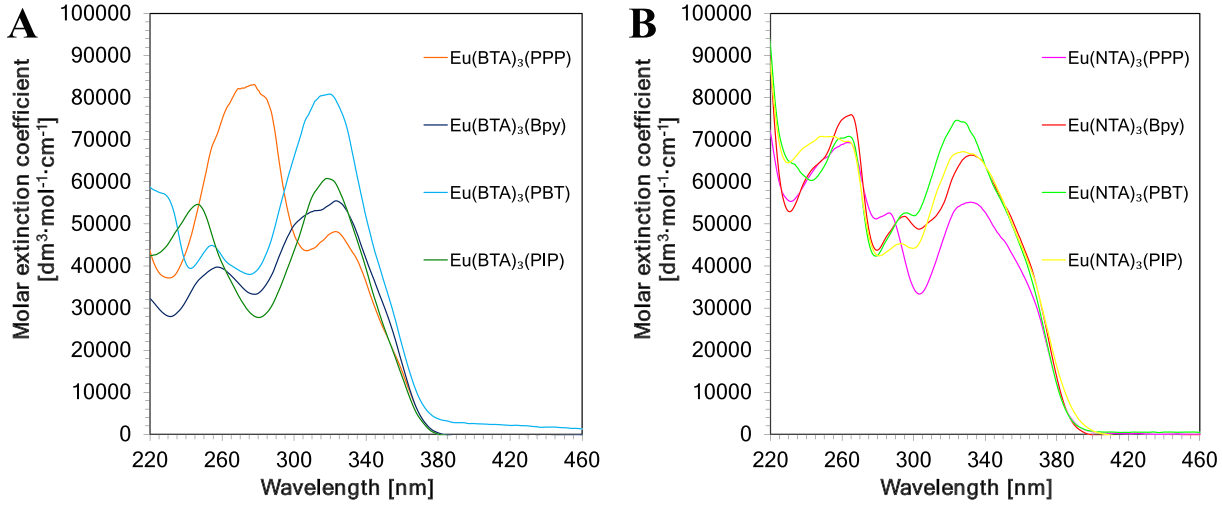


**Fig. 4.** UV–visible absorption spectra of the europium(III) complexes consist of the same diketone (**A**) (4,4,4-trifluoro-1-phenylbutane-1,3-dione) in acetonitrile and (**B**) (4,4,4-trifluoro-1-(2-naphthyl)butane-1,3-dione) in acetonitrile.

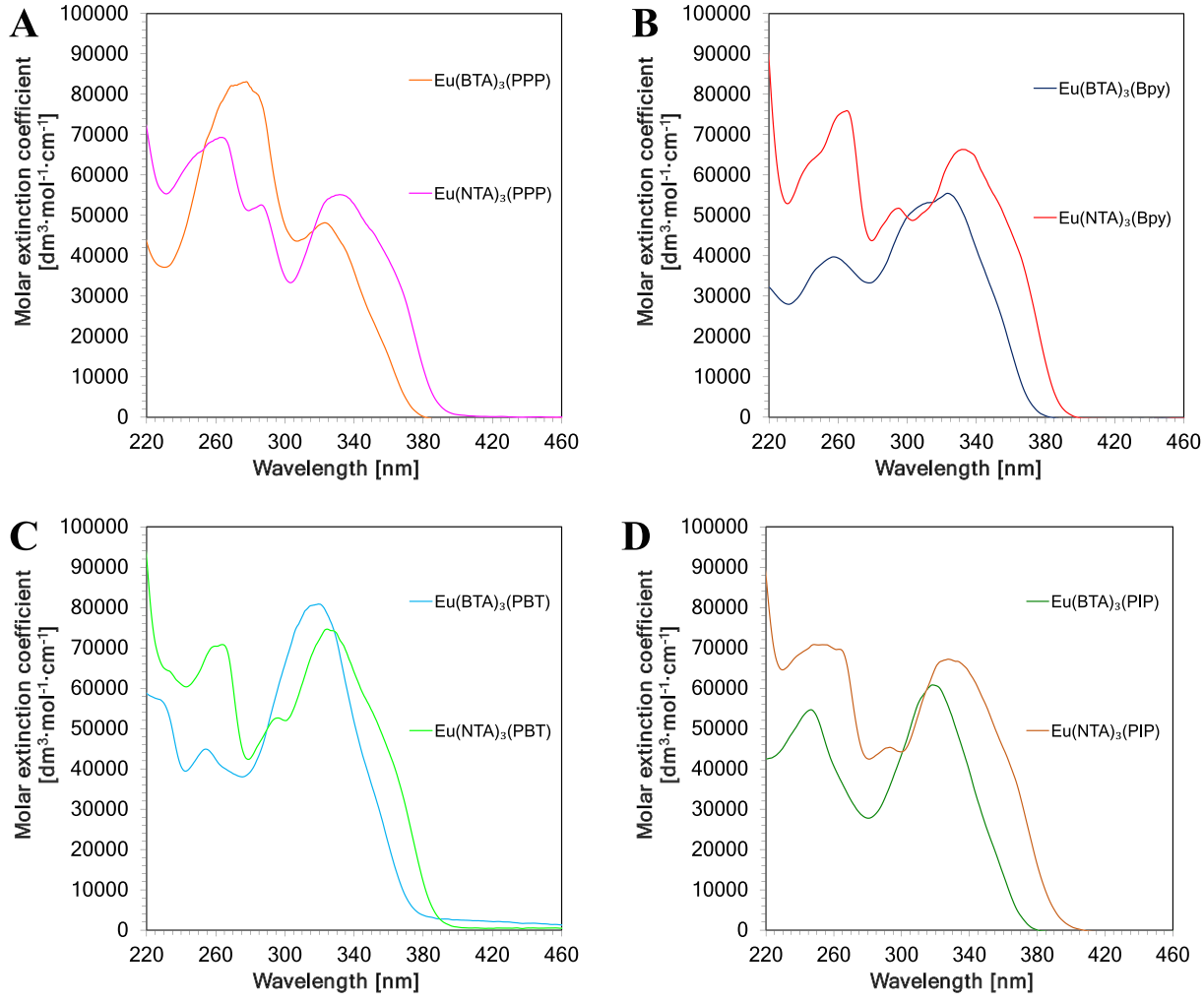


**Fig. 5.** UV–visible absorption spectra of the europium(III) complexes consist of the same stabilizing ligand (**A**) PPP in acetonitrile; (**B**) Bpy in acetonitrile; (**C**) PBT in acetonitrile and (**D**) PIP in acetonitrile.

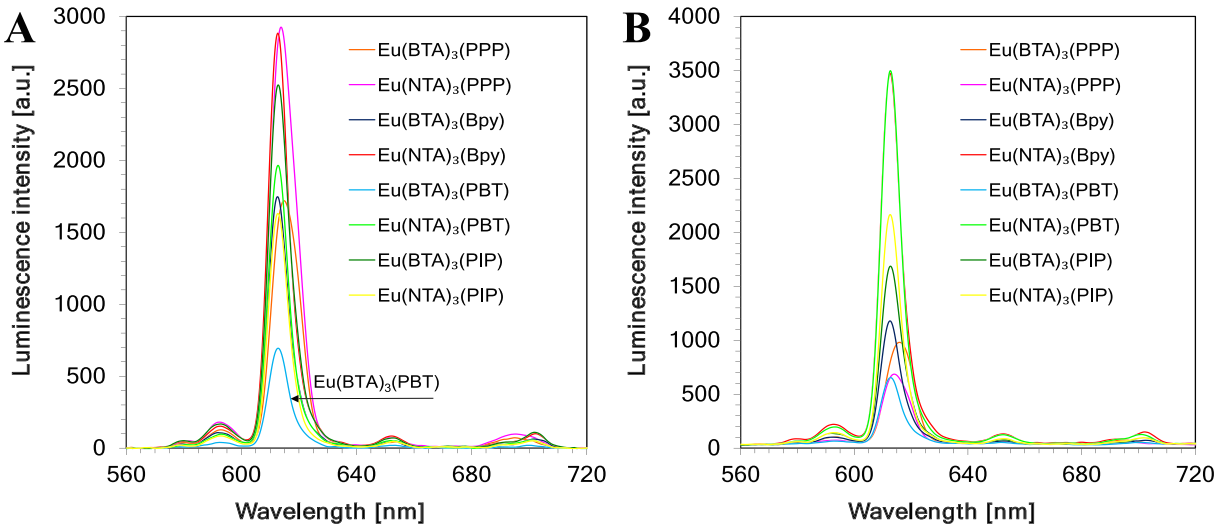


**Fig. 6.** Luminescence spectra of europium(III) complexes with acetonitrile (**A**) in excitation 320 nm and integration time 50 s; (**B**) acetonitrile in excitation 365 nm and integration time 400 s.

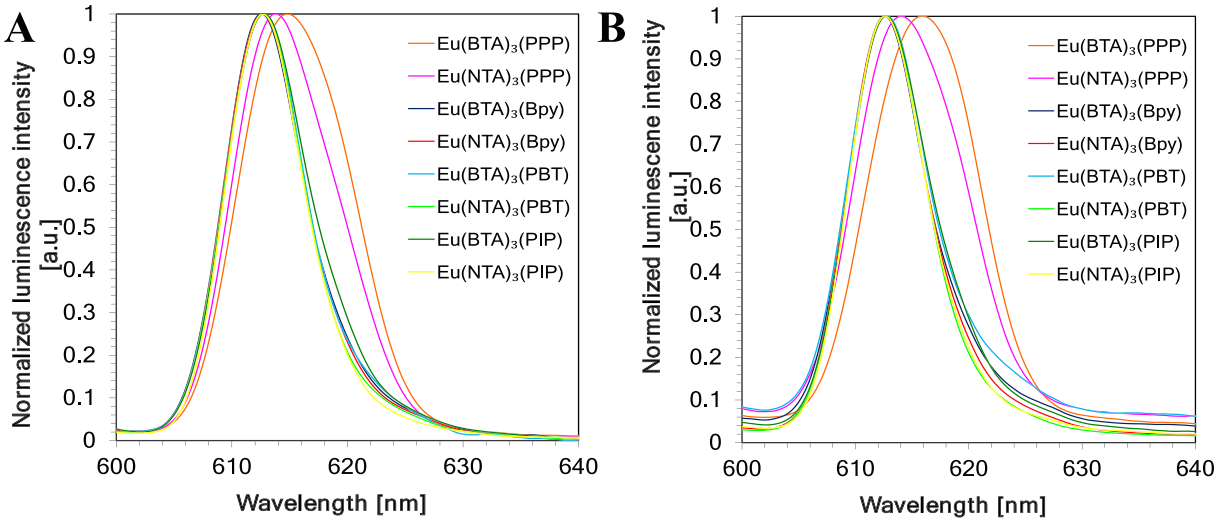


**Fig. 7.** Normalized luminescence spectra of europium(III) complexes with acetonitrile (**A**) in excitation 320 nm and integration time 50 s; (**B**) in excitation 365 nm and integration time 400 s.

### *3.2. Applicability of europium(III) complexes for monitoring cationic photopolymerisation*

#### *3.2.1. Changes of luminescence intensity upon cation photopolymerisation of TEGDVE monomer*

The potential application of the europium(III) complexes to monitor the cationic photopolymerisation using Fluorescence Probe Technology (FPT) has been discussed. For this purpose, the model monomer used for this purpose was triethylene glycol divinyl ether (TEGDVE), and the cationic photopolymerisation initiator was a commercially available - diphenyliodonium hexafluorophosphate (HIP). Measurements of changes in the intensity of luminescence spectra of europium(III) complexes compounds in the composition were made during the cationic photopolymerisation process of vinyl monomer. For measurements UV-LED diode with emission wavelength $\lambda_{max}$ = 320 nm was used. This diode was chosen as compatible with the absorption characteristics of the commercial photoinitiator diphenyldionium hexafluorophosphate (HIP) and the europium(III) complexes.

Following the results acquired from monitoring the changes in the intensity of luminescence spectra during the cationic photopolymerisation of the vinyl monomer (TEGDVE) process, a common trend was observed for all complexes (Figs. 8 and Fig. S9–S24). All of the complexes show a significant change in luminescence intensity. In each case, the luminescence intensity after the photopolymerisation process is lower than before this process. It is due to the partial decomposition of europium(III) complexes in direct relation to the release of a strong protic acid at the initiation stage, in this case, hexafluorophosphoric acid ($HPF_6$). The pH change to a strongly acidic environment negatively influences the europium(III) complexes occurring in the polymerisation composition. The generated strong protic acid contributes to the degradation of a significant part of these compounds. Therefore, the investigated europium(III) complex compounds have the potential to prove effective as an optical sensor for monitoring the first step of cationic photopolymerisation, i.e., initiation, and can probably provide information about the rate of protic acid generation during this process and can also give information about the released strength during the acid initiation step. To confirm these hypotheses, kinetic data of the cationic photopolymerisation process were conducted. According to the

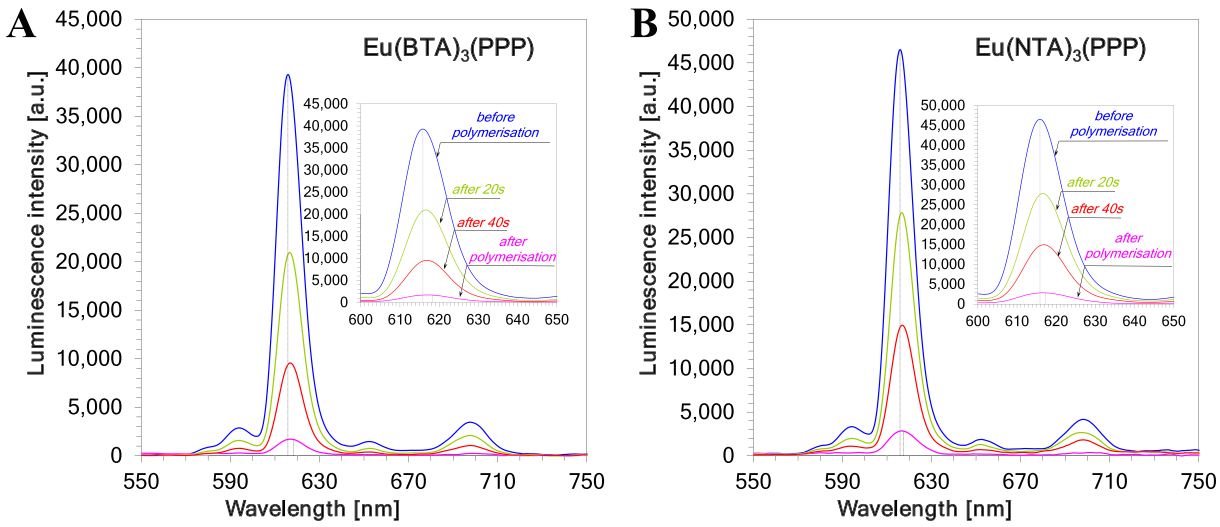


**Fig. 8.** Changes of luminescence spectra during cationic photopolymerisation of the TEGDVE monomer under irradiation of 320 nm for (**A**) $Eu(BTA)_3(PPP)$ and (**B**) $Eu(NTA)_3(PPP)$.

results, a significant decrease in luminescence intensity was observed in all complexes when monitoring the photopolymerisation of the vinyl monomer TEGDVE. The lowest luminescence intensity after the cationic photopolymerisation of vinyl monomer (TEGDVE) was observed for the compounds [(2-(2-pyridyl)imidazo[1,2-*a*]pyridine)tris(4,4,4-trifluoro-1-phenylbutane-1,3-dione)europium(III)] ($Eu(BTA)_3(PIP)$), and [(2-(2-pyridyl)imidazo[1,2-*a*]pyridine)tris(4,4,4-trifluoro-1-(2-naphthyl) butane-1,3-dione)europium(III)] ($Eu(NTA)_3(PIP)$), respectively $I_{max\text{-}A} = 759$ [a.u.] which is 99.0% of the initial value for $Eu(BTA)_3(PIP)$, and $I_{max\text{-}A} = 1413$ [a.u.] representing 98.0% of the initial value for Eu(NTA)3(PIP). Their structure is characterized with the same stabilizing ligand (PIP) and, respectively for $Eu(BTA)_3(PIP)$ diketone (4,4,4-trifluoro-1-phenylbutane-1,3-dione) (BTA) and for $Eu(NTA)_3(PIP)$ containing in its structure 44,4,4-trifluoro-1- (2-naphthyl) butane-1,3-dione) (NTA). This means that the least stable complexes are those made of a stabilizing ligand in the form of PIP.

Luminescence normalized intensity ($I_{max}/I_0$) found at the emission maximum at 614 nm peak was used as a parameter of photopolymerisation process progress. From Fig. 9, the stability of the studied europium(III) complexes to changes in environmental parameters during cationic photopolymerisation of the TEGDVE monomer can be established. However, it should be noted that the use of this parameter does not eliminate the influence of the thickness of the measuring layer on the acquired results, thus when using this parameter all measurements should be performed in one standard setting of instrumentation.

Moreover, depending on the type of substituents in the complexes, it was shown that these compounds exhibit different sensitivity and stability to the changes occurring during the cationic photopolymerisation of vinyl monomer, which can be determined by the parameter $I_{max}/I_0$. To compare in a quantitative way what kind of ligands in europium(III) complexes affect their sensitivity, the relative sensitivity of the obtained compounds was defined using the sensitivity parameter (S).

$$S = \frac{\left| \left(\frac{I_{max}}{I_0}\right)_{after} - \left(\frac{I_{max}}{I_0}\right)_{before} \right|}{\left(\frac{I_{max}}{I_0}\right)_{before}} \cdot 100\% \quad (2)$$

$(I_{max}/I_0)_{after} - (I_{max}/I_0)_{before}$ for the composition after the photopolymerisation.
$(I_{max}/I_0)_{before}$ – value $I_{max}/I_0$ for the composition before photopolymerisation

Furthermore, a sensitivity analysis of the obtained europium(III) complexes was performed, and an additional parameter of relative sensitivity was introduced, defining it as the ratio of the sensitivity value of the europium(III) complex to the sensitivity value of the most sensitive compound ($Eu(BTA)_3(Bpy)$). The list of acquired data is presented in Table 2. Analysis of the sensitivity value of europium(III) complexes leads to the conclusion that it is preferable to introduce a stabilizing ligand 2,2′-bipyridine (Bpy), into the structure, because $Eu(BTA)_3(Bpy)$, $Eu(NTA)_3(Bpy)$ complexes show the highest sensitivity. The introduction of other studied ligands such as 2-(2-pyridyl)-1,3-benzothiazole (PBT) and 2-(2-pyridyl)imidazo[1,2-*a*]pyridine (PIP), 4-phenyl-2,6-bis (2-pyridyl)pyridine (PPP) reduces sensitivity.

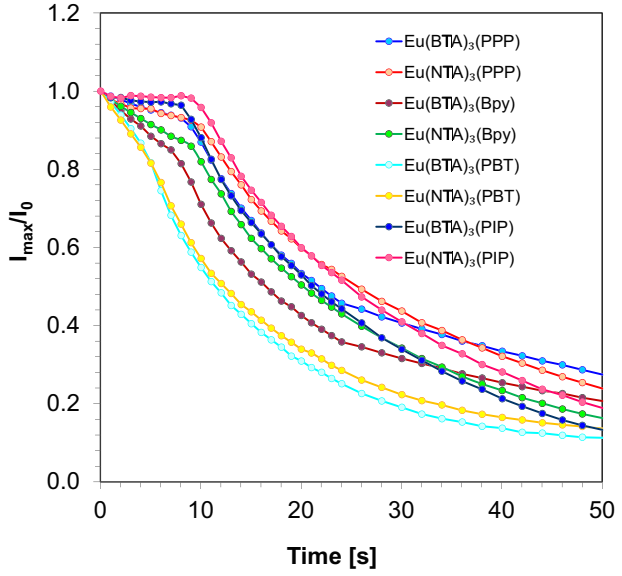


**Fig. 9.** Results of monitoring the cationic photopolymerisation of TEGDVE monomer under conditions 320 nm by FPT using the europium(III) complexes as fluorescent sensor and the $I_{max}/I_0$ parameter.

**Table 2**
Changes in luminescence spectra of the complexes after cationic photopolymerisation of TEGDVE monomer.

| Compound symbol | $\lambda_{max\text{-}B}$ [nm] | $I_{max\text{-}B}$ [a.u.] | $\lambda_{max\text{-}A}$ [nm] | $I_{max\text{-}A}$ [a.u.] | $\lvert\Delta I_{max}\rvert$ [a.u.] | $\Delta I_{max}$ [%] | $\Delta\lambda_{max}$ [nm] | $(dI_0/I_{max})/dt$ | t [s] | S | $S_{wzg}$ |
|---|---|---|---|---|---|---|---|---|---|---|---|
| $Eu(BTA)_3(PPP)$ | 616.9 | 46,535 | 617.3 | 2848 | 43,687 | 94 | 0.5 | 0.231 | 14.6 | 71.8 | 0.67 |
| $Eu(NTA)_3(PPP)$ | 616.9 | 39,308 | 618.2 | 1709 | 37,598 | 96 | 1.4 | 0.124 | 12.7 | 79.0 | 0.74 |
| $Eu(BTA)_3(Bpy)$ | 615.0 | 29,301 | 616.4 | 2230 | 27,071 | 92 | 1.4 | 0.197 | 12.2 | 107.5 | 1.00 |
| $Eu(NTA)_3(Bpy)$ | 614.6 | 36,144 | 616.4 | 2215 | 33,929 | 94 | 1.8 | 0.205 | 13.7 | 94.7 | 0.88 |
| $Eu(BTA)_3(PBT)$ | 615.0 | 19,880 | 616.9 | 1507 | 18,373 | 92 | 1.8 | 0.200 | 9.1 | 87.9 | 0.82 |
| $Eu(NTA)_3(PBT)$ | 615.0 | 22,229 | 616.4 | 2368 | 19,861 | 89 | 1.4 | 0.146 | 10.7 | 85.4 | 0.79 |
| Eu(BTA)3(PIP) | 615.0 | 56,878 | 617.1 | 759 | 56,119 | 99 | 2.1 | 0.619 | 13.8 | 89.8 | 0.83 |
| $Eu(NTA)_3(PIP)$ | 615.0 | 58,427 | 616.4 | 1413 | 57,014 | 98 | 1.4 | 0.304 | 11.6 | 85.1 | 0.79 |

$\lambda_{max\text{-}B}$ – position of the maximum luminescence before photopolymerisation process [nm].
$I_{max\text{-}B}$ – luminescence intensity for $\lambda_{max\text{-}B}$ [a.u.]
$\lambda_{max\text{-}A}$ – position of the maximum luminescence after photopolymerisation process [nm].
$I_{max\text{-}A}$ – luminescence intensity for $\lambda_{max\text{-}A}$ [a.u.]
$\lvert\Delta I_{max}\rvert = I_{max\text{-}before} - I_{max\text{-}after}$ – difference in luminescence intensity before and after the photopolymerisation process at $\lambda_{max\text{-}B}$ and $\lambda_{max\text{-}A}$, respectively [a.u.]
$\Delta I_{max}$ – relative change of luminescence intensity [%].
$\Delta\lambda_{max}$ – position of the maximum fluorescence before and after the photopolymerisation process [nm].
$(dI_0/I_{max})/dt$ – slope of the kinetic curve.
t – induction time [s].
S – sensitivity calculated based on Eq. (1).
$S_{wzg}$ – ratio of the sensitivity value of the europium(III) complex to the value of the most sensitive compound.

### 3.3. *Applicability of europium(III) complexes in free-radical photopolymerisation processes*

The possibility of application of europium(III) complexes as optical chemical sensors in photopolymerisation proceeding according to the radical mechanism was also investigated. As a photoinitiator of free radical polymerisation 2,2-dimethoxy-2-phenylacetophenone (OMEGA) was proposed. The behaviour of the studied europium(III) complexes was checked in the acrylic trimethylolpropane triacrylate monomer (TMPTA). Monitoring of the free -radical photopolymerisation process was carried out using UV light with a maximum wavelength of 320 nm for all europium(III) complexes in acrylic monomer (TMPTA). For these purposes, the solutions consisted of appropriate europium(III) complexes with molar concentrations in the range $1.06 \cdot 10^{-5}$–$9.65 \cdot 10^{-6}$ mol/L, which accounted for 0.1% by weight relative to the whole mixture and the photoinitiator - OMEGA with concentration of 1% by weight were prepared. An analysis of changes in the intensity of luminescence spectra for europium(III) complexes with the TMPTA monomer was carried out during the free-radical photopolymerisation process. During the irradiation of the europium(III) complex compounds, it was observed that they showed a maximum emission in the range of 612–616 nm. Based on Figs. 10; S25–S30 and Table 3 showing the dependence of the change in luminescence intensity on the wavelength, it can be stated that the highest luminescence intensity after the polymerisation process in acrylic monomer (TMPTA) is achieved by [(2,2′-bipyridine)tris(4,4,4-trifluoro-1-(2-naphthyl)butane-1,3-dione)europium(III)] ($Eu(NTA)_3(Bpy)$) (3953 [a.u.]), On the other hand the lowest value of luminescence intensity after the polymerisation process is [4-phenyl-2,6-bis(2-pyridyl)pyridine)tris (4,4,4-trifluoro-1-phenylbutane-1,3-dione)europium(III)] ($Eu(BTA)_3(PPP)$) (329 [a.u.]), which in its structure has 4-phenyl-2,6-bis(2-pyridyl)pyridine (PPP) as a stabilizing ligand and a (4,4,4-trifluoro-1-phenylbutane-1,3-dione)europium(III) (BTA). Europium(III) complexes do not show any shift in the luminescence spectrum during the photopolymerisation process of the acrylic TMPTA monomer. Only $Eu(BTA)_3(PPP)$ shows a very negligible luminescence shift at 614 nm of only 0.3 [nm]. For this reason, the idea was born to study the obtained compounds as sensors for determining the thickness of polymer coatings. Table 3 summarizes the most important parameters of the recorded luminescence band at maximum emission is presented.

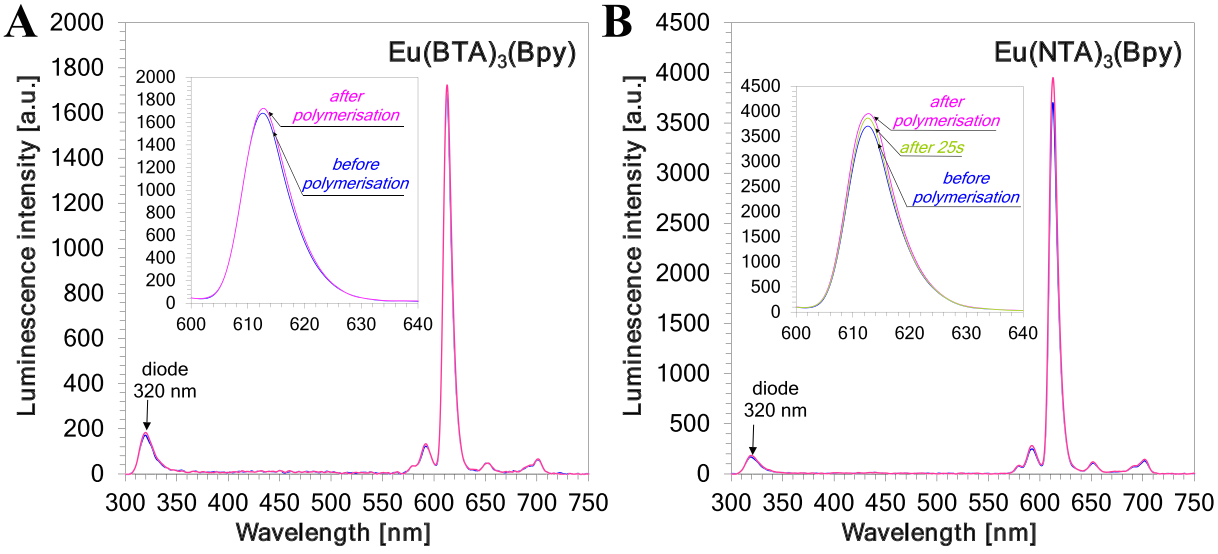


**Fig. 10.** Changes of luminescence spectra during free-radical photopolymerisation of the TMPTA monomer (**A**) under irradiation of 320 nm for $Eu(BTA)_3(Bpy)$ and (**B**) under irradiation of 320 nm for $Eu(NTA)_3(Bpy)$.

**Table 3**
Changes of luminescence spectra of the complexes studied upon free-radical photopolymerisation of TMPTA monomers.

| Compound symbol | $\lambda_{max\text{-}B}$ [nm] | $I_{max\text{-}B}$ [a.u.] | $\lambda_{max\text{-}A}$ [nm] | $I_{max\text{-}A}$ [a.u.] | $\lvert\Delta I_{max}\rvert$ [a.u.] | $\Delta I_{max}$ [%] | $\Delta\lambda_{max}$ [nm] |
|---|---|---|---|---|---|---|---|
| $Eu(BTA)_3(PPP)$ | 613.9 | 399 | 614.2 | 329 | 70 | 17.5 | 0.3 |
| $Eu(NTA)_3(PPP)$ | 614.5 | 2978 | 614.5 | 3272 | 294 | −9.9 | 0 |
| $Eu(BTA)_3(Bpy)$ | 612.7 | 1681 | 612.7 | 1724 | 43 | −2.6 | 0 |
| $Eu(NTA)_3(Bpy)$ | 612.7 | 3703 | 612.7 | 3953 | 250 | −6.8 | 0 |
| $Eu(BTA)_3(PBT)$ | 613.0 | 3694 | 613.0 | 3468 | 226 | 6.1 | 0 |
| $Eu(NTA)_3(PBT)$ | 613.0 | 2644 | 613.0 | 2726 | 82 | −3.1 | 0 |
| Eu(BTA)3(PIP) | 612.7 | 2765 | 612.7 | 2798 | 33 | −1.2 | 0 |
| $Eu(NTA)_3(PIP)$ | 612.7 | 2255 | 612.7 | 2429 | 174 | −7.7 | 0 |

$\lambda_{max\text{-}B}$ – position of the maximum luminescence before the photopolymerisation process [nm].
$I_{max\text{-}B}$ – luminescence intensity for $\lambda_{max\text{-}B}$ [a.u.]
$\lambda_{max\text{-}A}$ – position of the maximum luminescence after photopolymerisation process [nm].
$I_{max\text{-}A}$ – luminescence intensity for $\lambda_{max\text{-}A}$ [a.u.]
$\lvert\Delta I_{max}\rvert = I_{max\text{-}before} - I_{max\text{-}after}$ – difference in luminescence intensity before and after the photopolymerisation process at $\lambda_{max\text{-}B}$ and $\lambda_{max\text{-}A}$, respectively [a.u.]
$\Delta I_{max}$ – relative change of luminescence intensity [%].
$\Delta\lambda_{max}$ – position of the maximum fluorescence before and after the photopolymerisation process [nm].

### *3.4. Influence of polymer composition thickness on the free-radical photopolymerisation process*

The effect of thickness measurements of polymeric composition during free-radical photopolymerisation on the luminescence intensity of selected europium(III) complexes was studied. Four europium(III) complexes were selected to investigate the thickness of the fabricated compositions. The first compound used for this analysis was the Eu $(NTA)_3(PPP)$ complex, containing 4-phenyl-2,6-bis(2-pyridyl)pyridine in its structure. The next compound selected for studies on the

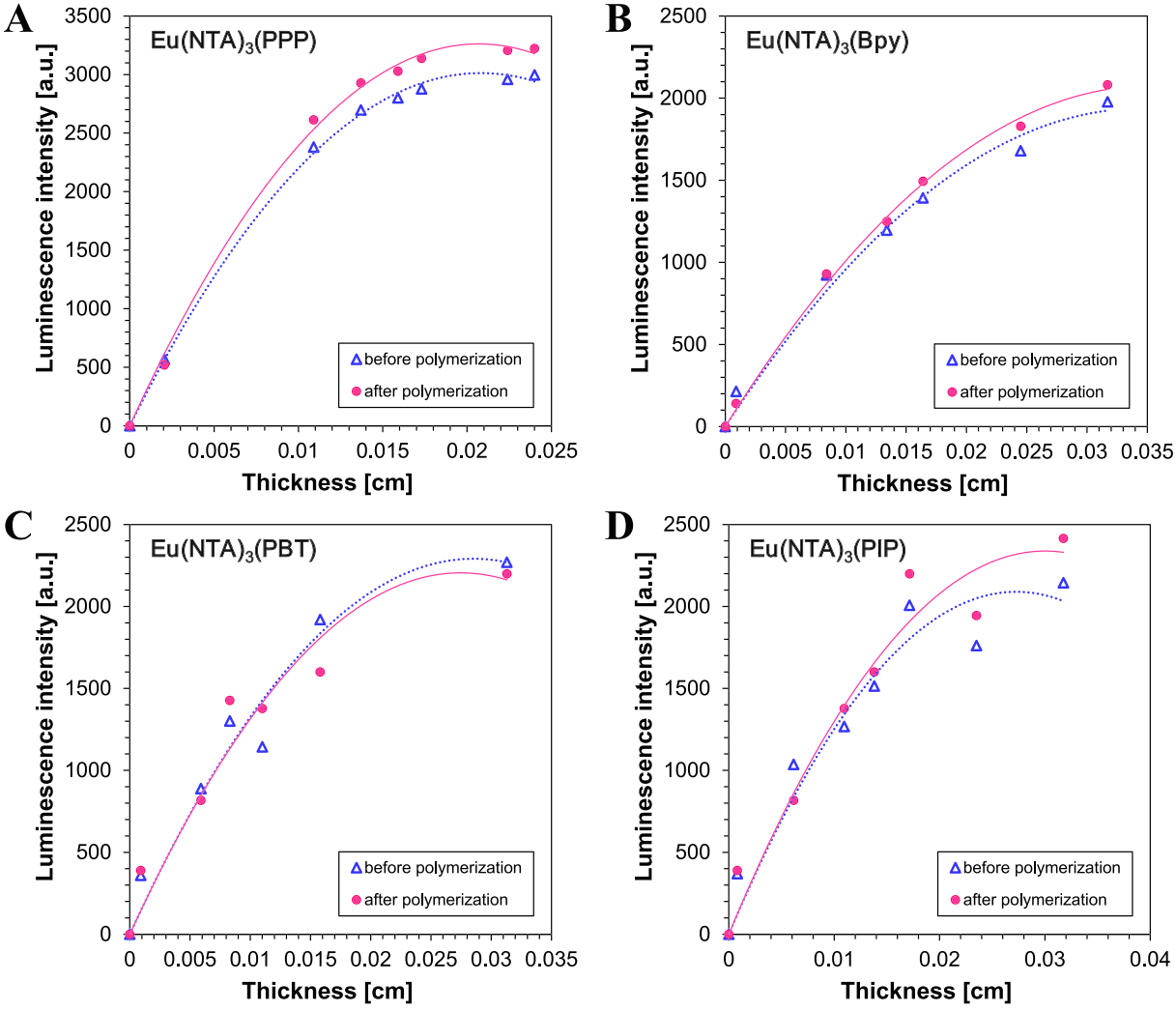


**Fig. 11.** Dependence of luminescence intensity on coating thickness (**A**) for $Eu(NTA)_3(PPP)$ complexes before and after photopolymerisation of TMPTA monomer; (**B**) for $Eu(NTA)_3(Bpy)$ complex before and after photopolymerisation of TMPTA monomer; (**C**) thickness for $Eu(NTA)_3(PBT)$ complex before and after photopolymerisation of TMPTA monomer and (**D**) for $Eu(NTA)_3(PIP)$ complex before and after photopolymerisation of TMPTA monomer.

thickness of the obtained compositions was the Eu(NTA)$_3$(Bpy) complex. Its structure is characterized by the content of a diketone substituent with a naphthyl group conjugated to a stabilizing ligand, which was 2,2′-bipyridine. The third compound selected for testing the layer thickness of the obtained compositions was Eu(NTA)3(PBT). Its structure is characterized by the content of the diketone substituent and the presence of a stabilizing ligand, which was 2-(2-pyridyl)-1,3-benzothiazole. The last compound selected for the study of the thickness was the Eu(NTA)$_3$(PIP) complex. Its structure is characterized by the content of a stabilizing ligand, which was 2-(2-pyridyl)imidazo[1,2-*a*]pyridine.

Micrometre screw gauge was used to prepare precise layers with a precisely defined coating thickness. Moreover, all of the measurement parameters, such as the excitation light intensity and excitation wavelength, europium(III) complex concentration, geometric measurement parameters, etc. were kept constant. The thickness of the sample was changed from 0.01 mm to 0.35 mm using different spacers.

A series of measurements using Fluorescence Probe Technology was carried out after exposing the measuring system to a UV-LED diode emitting radiation with wavelength $\lambda_{max} = 320$ nm in order to evaluate the possibility of using selected europium(III) complexes as thickness sensors. Fig. 11 shows the relationship between the thickness of the polymer sample and the luminescence intensity of the complexes emitted both before the photopolymerisation process (blue line) and after the photopolymerisation process (pink line). In Fig. 12, the relationship between luminescence intensity and coating thickness is nonlinear with probe concentration. It can be considered linear only at small thicknesses, below 5 μm. This nonlinearity is due to the fact that the intensity of the excitation light decreases along the coating thickness as a result of light absorption. Less luminescence intensity is generated from layers far from the coating surface than near the illuminated surface.

Fortunately, the exact relationship between luminescence intensity ($I_L$) and coating thickness (b) can be expressed by Eq. (3).

$$I_L = k \cdot \phi_L \, I_0 \cdot \left(1 - 10^{-\varepsilon_L \cdot b \cdot C_L}\right) \tag{3}$$

where:

k - proportionality coefficient
$\phi_L$ - luminescence efficiency
$I_0$ - the incident light intensity [a.u.]

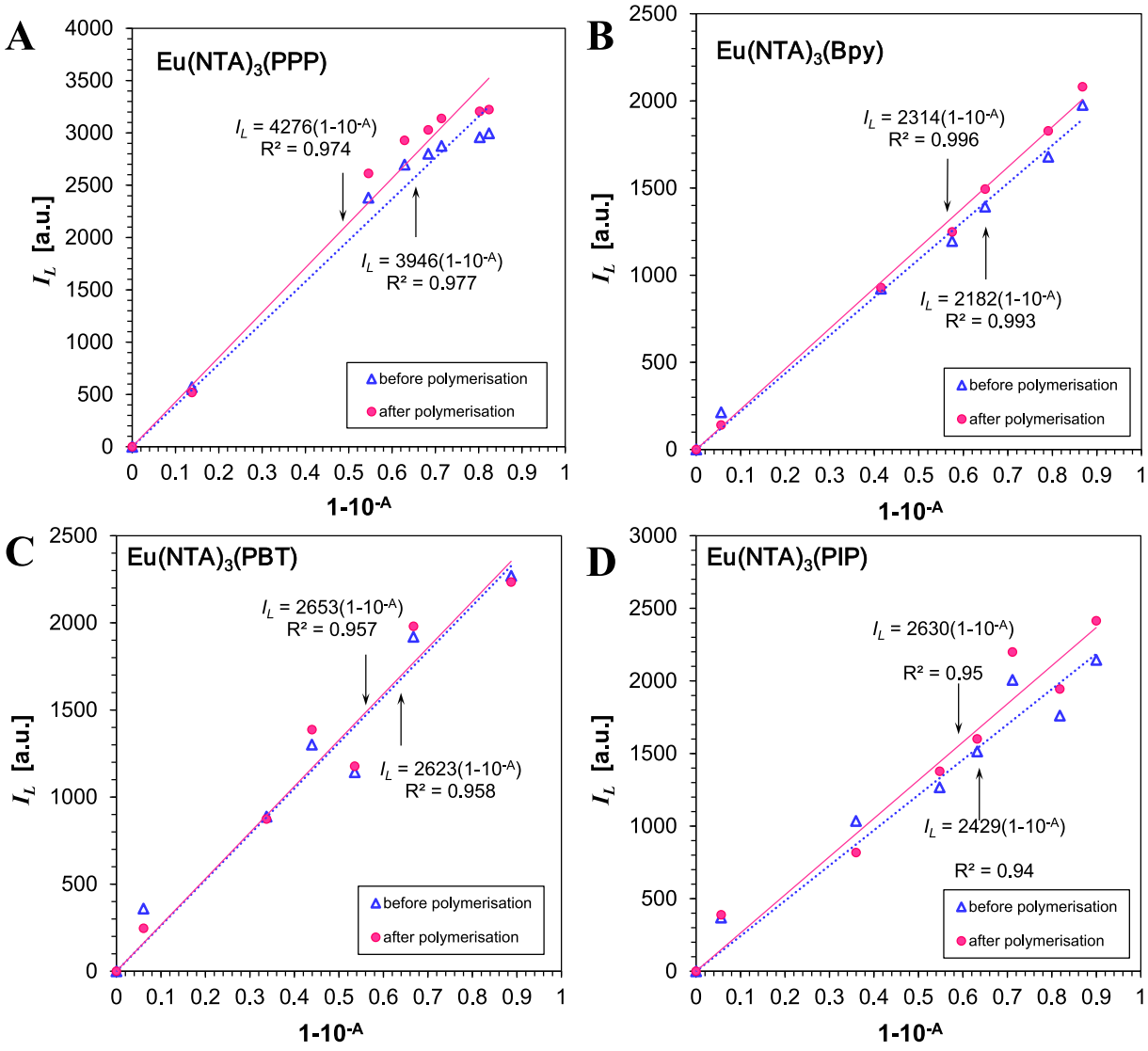


**Fig. 12.** Dependence of luminescence intensity ($I_L$) on the fraction of light intensity absorbed by the sample ($1–10^{-A}$) (**A**) for Eu(NTA)$_3$(PPP) complex in TMPTA monomer; (**B**) for Eu(NTA)$_3$(Bpy) complex in TMPTA monomer; (**C**) for Eu(NTA)$_3$(PBT) complex in TMPTA monomer (**D**) for Eu(NTA)$_3$(PIP) complex in TMPTA monomer.

$\varepsilon_L$ - extinction coefficient of the luminescing species at the excitation wavelength, in [$dm^3$ $mol^{-1}$ $cm^{-1}$],
$C_L$ - molar concentration of the luminescing species in [mol $dm^{-3}$].

Thus, at constant probe concentration ($C_L$), constant excitation light intensity ($I_0$), and constant measurement conditions (i.e., the same k) where the absorbance (A) gets low, the luminescence intensity ($I_L$) is a linear function of the coating thickness (b)

$$I_L \cong (2.303k \cdot I_0 \cdot \varepsilon_L \cdot C_L) \cdot b \quad (4)$$

In order to verify the correctness of the general Eq. (3) at high absorbances, the absorbance of europium(III) complexes was calculated at 320 nm (which was the dominant wavelength of light emitted by the UV diode used).

The measurements made it possible to correlate the thickness of the polymer coating with the luminescence of the sensor, taking into account the absorption level of the studied complexes in the TMPTA monomer and based on Lambert-Beer's law a curve between 1 and $10^{-A}$ and the metal emission intensity was plotted. The luminescence intensities measured for different sample thicknesses and plotted as a function of 1–$10^{-A}$ are shown in Fig. 12. In each case, a linear dependence of luminescence intensity on 1–$10^{-A}$ was obtained for all europium(III) complexes tested with a high correlation coefficient above 0.95 at least 7 data points.

The complex compounds Eu(NTA)$_3$(PPP), Eu(NTA)$_3$(Bpy), Eu(NTA)$_3$(PBT) and Eu(NTA)$_3$(PIP) presented above, as well as all others, which show low variability of the luminescence intensity parameter at the maximum emission of 614 nm during free-radical photopolymerisation processes can be added to various compositions. After applying the sample and measuring its luminescence, information about the thickness of its coating is obtained without measuring the thickness with specialized equipment.

Another application of the europium(III) complex is their use as internal markers for organic probes to make the measurement independent of sample thickness. Based on the obtained results, it can be seen that the same trend remains during the measurements. Namely, the europium(III) complexes can serve as internal markers, because regardless of whether the spectra presented above are before the photopolymerisation process or after the photopolymerisation process, the trend is stabled. The europium (III) complexes can be applied as potential internal probes. They can be used as probes due to luminescence stability during free-radical photopolymerisation and lack of luminescence spectrum shift during the process.

### 3.5. Mechanism of the europium(III) complexes during cationic photopolymerisation

Encouraged by these interesting results, the experiments were subsequently carried out, which should explain the decrease in luminescence intensity during the cationic photopolymerisation of TEGDVE monomer and the stability of europium complexes during radical photopolymerisation (Figs. 13 and S39–45).

For this purpose, four different compositions were prepared and measured by FPT techniques. The first sample was the standard photocurable composition based on fluorescent sensors - [4-phenyl-2,6-bis (2-pyridyl)pyridine)tris(4,4,4-trifluoro-1-phenylbutane-1,3-dione) europium(III)] (Eu(BTA)$_3$(PPP)), the diphenyliodonium hexafluorophosphate photoinitiator and triethylene glycol divinyl ether as vinyl monomers (sensor/HIP/TEGDVE); the second sample had sensors dissolved in only vinyl monomer (sensor/TEGDVE); the third sample was based on the investigated sensor with the cationic photoinitiator dissolved in the non-reactive monomer polyethylene glycol diacrylate (sensor/HIP/PEGDA200); and the fourth composition consisted of only the sensor Eu(BTA)$_3$(PPP) and the monomer polyethylene glycol diacrylate (Fig. 14).

The first composition, probe/HIP/TEGDVE is a standard composition

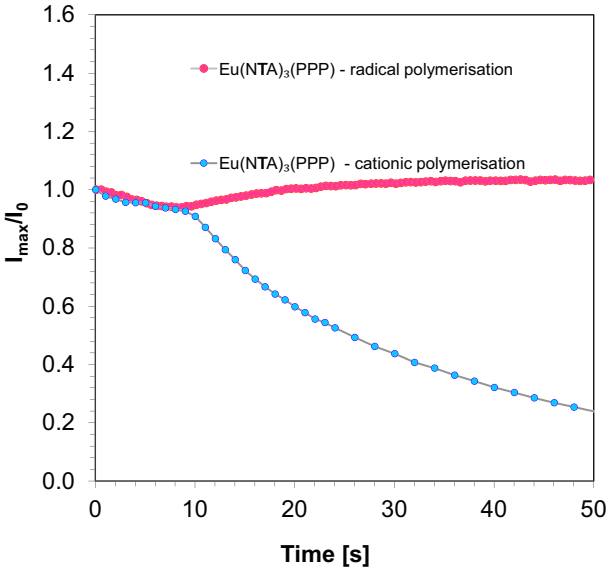


**Fig. 13.** Results of monitoring the cationic photopolymerisation of TEGDVE monomer and TMPTA monomer under conditions 320 nm by FPT using the Eu(NTA)$_3$(PPP) as a fluorescent sensor and the $I_{max}/I_0$ parameter.

used for monitoring the measurements of the kinetics of the cationic photopolymerisation process. The second composition did not contain a photoinitiator, iodonium salt, and thus the composition could not polymerize. The third composition contained the HIP photoinitiator and the non-reactive monomer PEGDA200. In this case, the composition cannot be polymerized due to the lack of a reactive monomer. The fourth composition is consisted only of the sensor and the non-reactive PEGDA 200 monomer. All four types of compositions were irradiated with a UV-LED diode with a maximum emission of 320 nm (1 mW $cm^{-2}$) for 100 s. In the case where no photoinitiator was used (sensor/TEGDVE and sensor/PEGDA200) a slight decrease in the luminescence intensity of the europium complex was observed, which is directly caused by the slight photolysis of the europium complex. When the irradiating composition consisting of (sensor/HIP/PEGDA200) the decrease in luminescence intensity was observed. During this process, the polarity and viscosity of the system did not change (Figs. 14–15). Therefore, the changes in emission spectra had to be caused by the release of a strong protic acid from the diphenyliodonium hexafluorophosphorane (HIP) photoinitiator during exposure, the photoinitiator photocleaved according to a previous report [24].

The change in the luminescence intensity of the europium complexes with the addition of the HIP photoinitiator can be explained by the formation of keto and enol forms of dicarbonyl groups in the europium complexes depending on the pH. It is known that the complexation of carbonyl groups with rare earth metals is difficult and depends on the pH and the concentration of the buffer. Dicarbonyl groups in europium complexes exist as an equilibrium between keto and enol forms depending on the solvent and pH [67]. In acidic solutions, the ketone form prevails and complexation is not possible. As the pH increases, complexation is easier but depends on the buffer concentration.

Fig. 16 shows the kinetic profiles of the composition consisting of sensor/HIP/TEGDVE and sensor/HIP/PEGDA200 after reducing the effect of the photolytic decomposition of the sensor by irradiating it with a UV-LED diode with a maximum emission of 300 nm. For this purpose, it was assumed that the decrease in the luminescence intensity of the Eu(BTA)$_3$(PPP) sensor in the last 20 s of the process results only from the photolysis of the sensor. Then, with the help of appropriate kinetic models of the photolysis reaction and based on the basic dependencies characterizing the phenomenon of luminescence, the change in luminescence intensity caused by the phenomenon of photolytic sensor

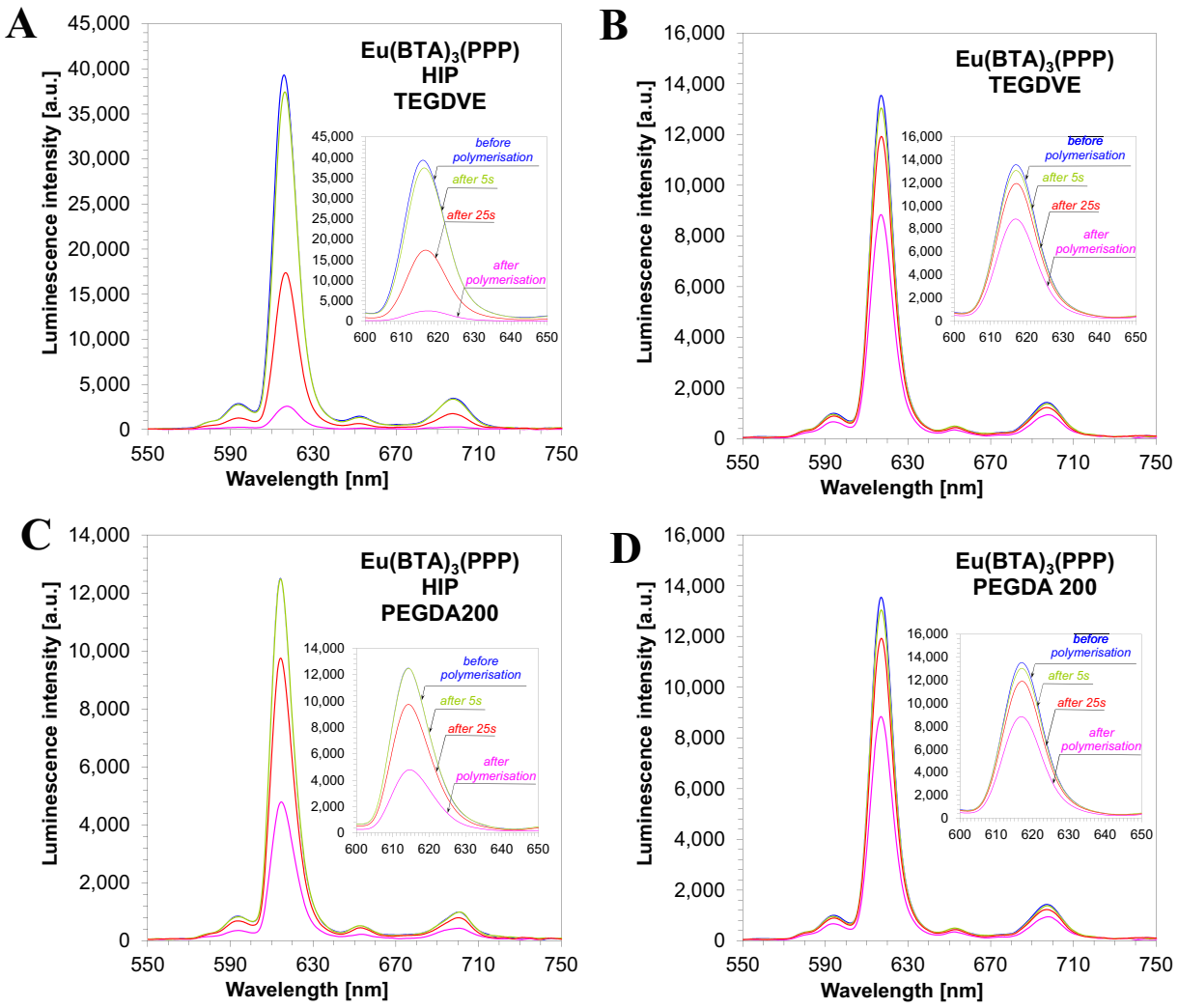


**Fig. 14.** Changes of luminescence spectra during free-radical photopolymerisation of the TMPTA monomer (**A**) under irradiation of 320 nm for Eu(BTA)$_3$(PPP)/HIP/TEGDVE (**B**) under irradiation of 320 nm for Eu(BTA)$_3$(PPP)/TEGDVE and (**C**) under irradiation of 320 nm for Eu(BTA)$_3$(PPP)/HIP/PEGDA200 (**D**) under irradiation of 320 nm for Eu(BTA)$_3$(PPP)/PEGDA200.

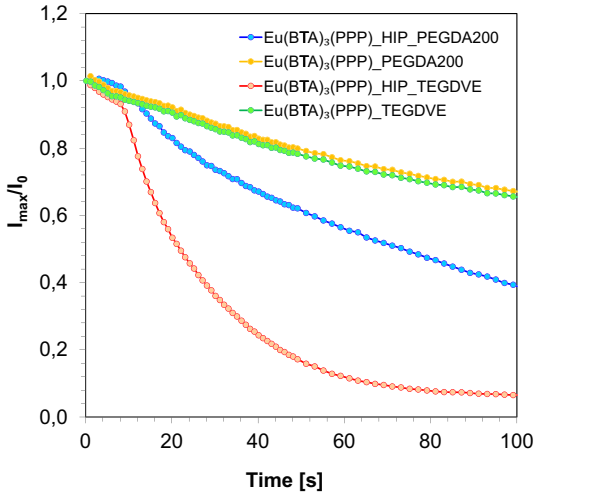


**Fig. 15.** Results of monitoring the cationic photopolymerisation of TEGDVE or PEGDA200 monomers under conditions 320 nm by FPT using the Eu(BTA)$_3$(PPP) as a fluorescent sensor and the $I_{max}/I_0$ parameter.

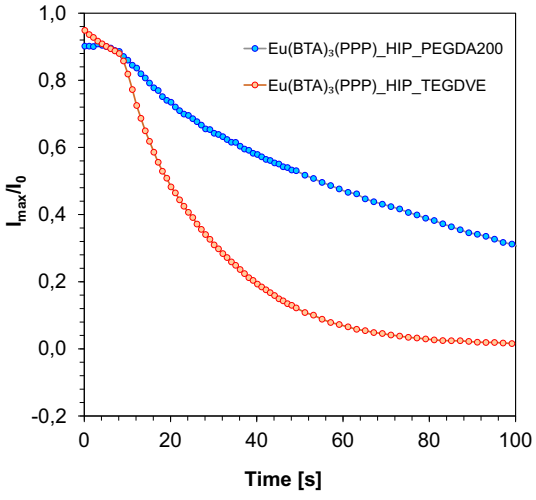


**Fig. 16.** Results of monitoring the cationic photopolymerisation of TEGDVE or PEGDA200 monomers under conditions 320 nm by FPT using the Eu(BTA)$_3$(PPP) as a fluorescent sensor and the $I_{max}/I_0$ parameter after reducing the photolysis effect.

decay as a function of the time of exposure of the sample to ultraviolet light was determined. The reasoning and the corresponding mathematical transformations for the photolysis process are presented below.

Photolysis as a first-order reaction can be described by the kinetic Eq. (5):

$$-\frac{d[S]}{dt} = k\,[S] \tag{5}$$

By dividing the variables, Eq. (6) is obtained

$$-\frac{1}{[S]}d[S] = kdt \tag{6}$$

After integration, the dependence of the concentration of the sensor in the sample on the time of the photolysis process is obtained (the time of the photolysis process was further assumed to be equal to the exposure time of the sample) (Eq. (7)):

$$-ln[S] = kt \tag{7}$$

$$[S] = exp\,(-kt) \tag{8}$$

On the other hand, the dependence of the sensor emission intensity as a function of its concentration can be described by the following relations:

$$I = k\left(1 - 10^{-A}\right) \tag{9}$$

$$A = \varepsilon lc \tag{10}$$

where:

A – absorbance.
$\varepsilon$ – molar absorbance coefficient [$dm^3\ mol^{-1}\ cm^{-1}$].
l – layer thickness [cm].
c – sensor concentration [$mol/dm^3$].

The determined dependence of the probe concentration on the emission intensity is as follows:

$$[S] = c = \left(\frac{log\left(1 - \frac{I}{k}\right)}{-\varepsilon l}\right) \tag{11}$$

For the sake of simplicity, it can be assumed that the dependence of the sensor concentration [S] on the sensor emission intensity can be described by the following equation:

$$[S] = kl \tag{12}$$

Substituting the above equation into the relationship $\ln[S] = -kt$

$$ln(k_1 l) = -Kt \tag{13}$$

By introducing the sensor emission intensity at time $t = 0$ [s], the following is obtained:

$$ln\frac{k_1 I}{k_2 I_0} = -Kt \tag{14}$$

$$ln\left(\frac{I}{I_0}\right) = -Kt - ln\left(\frac{k_1}{k_2}\right) \tag{15}$$

Meaning $-K = b$; $-ln\left(\frac{k_1}{k_2}\right) = a$

$$ln\left(\frac{I}{I_0}\right) = a + bt \tag{16}$$

$$\frac{I}{I_0} = exp(a + bt) \tag{17}$$

whereby for t = 0 [s]: $\rightarrow \frac{I}{I_0} = 1 \rightarrow a = 0$.

Due to the slight changes in the luminescence of the sensor due to the polymerisation of the composition (change in viscosity, polarity), the slope of the curve (coefficient b) was determined using the Eq. (14). Eq. (14) was a linear fit for the coefficient $a \neq 0$, and then it was reduced to a value equal to 0.

In the time interval from 80 s to 100 s of exposure to the sample, on the basis of the known values of ln ($I/I_0$), the value of the coefficient b in the equation (Eq. (16), for each of the tested samples) was determined. Then, based on Eq. (17), assuming the coefficient $a = 0$, the change of luminescence caused by sensor photolysis was determined for the entire time range of exposure of the sample (from 0 s to 100 s). By mathematically subtracting the kinetic profiles of the photolysis reaction from the temperature profiles of the photopolymerisation reaction, the exact temperature profiles of the photopolymerisation reaction were obtained after the compensation of the photolysis effect of the sensor, which is shown in Fig. 16.

After the mathematical reduction of the photolysis effect, it can be observed that the blue profile is responsible only for the release of a strong protic acid from the HIP photoinitiator.

### 3.6. Europium complexes as the "naked eye" sensor to monitor cationic photopolymerisation

The next stage of the research was to carry out the cationic photopolymerisation process using the Real-Time FT-IR technique. For this purpose, a composition consisting of $Eu(BTA)_3(PPP)$/HIP/TEGDVE was irradiated with a UV-LED diode with a maximum wavelength of 300 nm.

A significant decrease in the luminescence intensity of the studied europium complex during cationic photopolymerisation can be used to monitor the degree of hardening of the polymer coating. During the cationic photopolymerisation process, a change in the colour of the europium complex from red to orange (after 10 s), pink (after about 300 s) to complete photobleaching of the composition (after 900 s) is observed. After complete curing (90% conversion), complete photobleaching of the europium complex were observed (Fig. 17). Therefore, this complex can be used as a "naked eye" sensor to determine the degree of coating polymerisation.

On the other hand, it is worth noting that the europium complexes are stable in the TMPTA monomer. No significant colour changes of the europium complexes were observed during exposure of the composition consisting of the europium complex, OMEGA initiator, and TMPTA monomer (Fig. 18). Therefore, these complexes can be used as sensors for the thickness of polymer coatings on acrylate monomers.

## 4. Conclusion

Herein, novel europium(III) complexes suitable as molecular probes for monitoring the cationic photopolymerisation of the vinyl monomer TEGDVE have been reported. During this process, no shift in the emission spectrum has been observed, but only a decrease in the luminescence intensity. Therefore, monitoring of the photopolymerisation process of the TEGDVE monomer is possible using the $I_{max}/I_0$ parameter, found at the emission maximum corresponding to the transition between $^5D_0$-$^7F_2$. Furthermore, these probes are primarily responsive to the concentration of acid generated during photoinitiation, while changes in the polarity and viscosity of the medium have only a minor effect on the intensity of the luminescence spectra.

Finally, in this paper, the application of europium(III) complexes as polymer coating thickness sensors in the free radical photopolymerisation of TMPTA monomer using FPT technology has been introduced. Therefore, the results presented in this paper extend their potential application to the coating industry involving destructive and waste-generating methods.

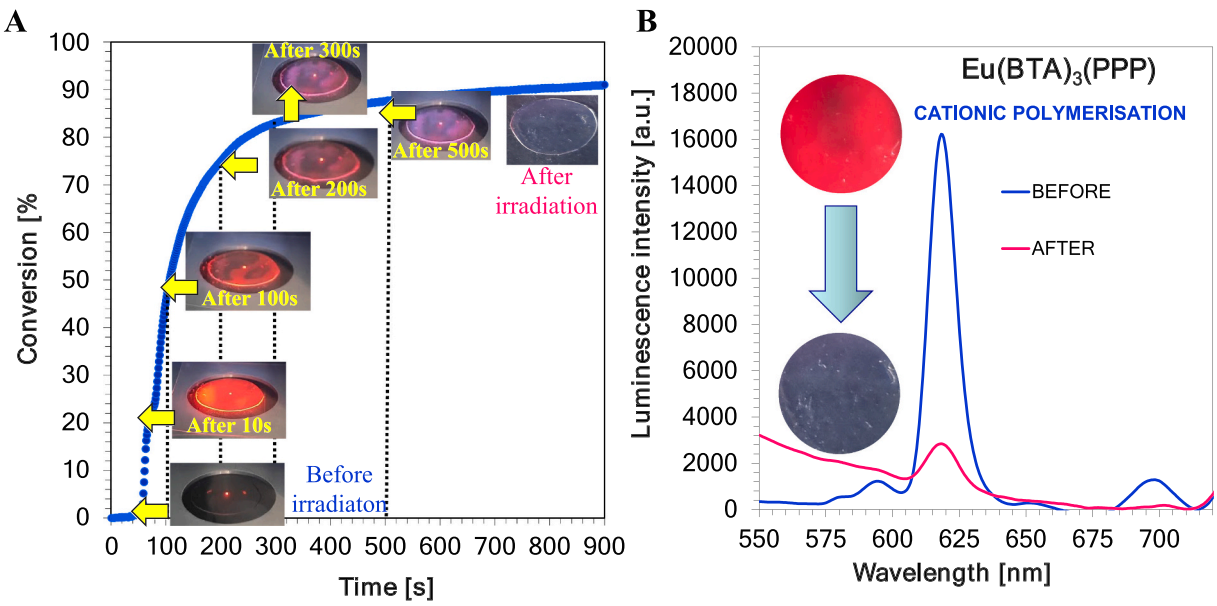


**Fig. 17.** (**A**) Polymerisation profiles of TEGDVE (vinyl function conversion vs. irradiation time) upon exposure to the UV LED@300 nm (0.5 mW $cm^{-2}$) in laminate in the presence of $Eu(BTA)_3(PPP)$/HIP/TEGDVE (**B**) Luminescence spectra of $Eu(BTA)_3(PPP)$/HIP/TEGDVE before and after cationic photopolymerisation.

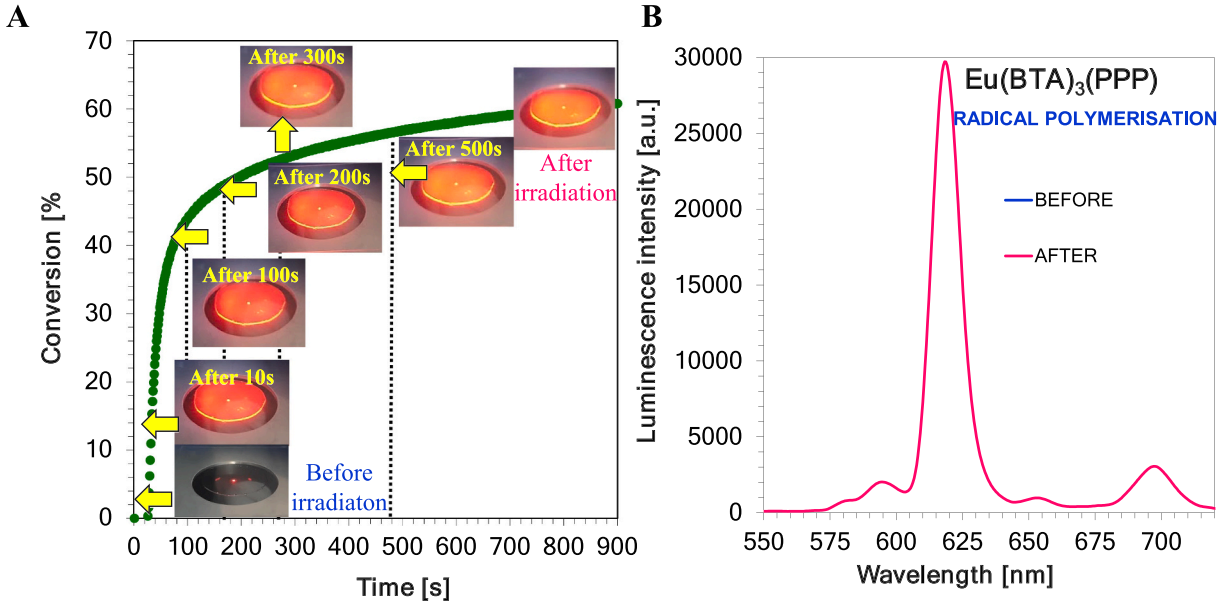


**Fig. 18.** (**A**) Polymerisation profiles of TMPTA (acrylate function conversion vs. irradiation time) upon exposure to the UV LED@300 nm (0.5 mW $cm^{-2}$) in laminate in the presence of $Eu(BTA)_3(PPP)$/HIP/TEGDVE (**B**) Luminescence spectra of $Eu(BTA)_3(PPP)$/HIP/TEGDVE before and after radical photopolymerisation.

## CRediT authorship contribution statement

**Monika Topa:** Conceptualization, Validation, Formal analysis, Investigation, Data curation, Writing – original draft, Writing – review & editing, Visualization. **Anna Chachaj-Brekiesz:** Formal analysis, Investigation, Data curation. **Tomasz Świergosz:** Validation, Writing – review & editing, Visualization. **Roman Popielarz:** Conceptualization, Methodology, Software, Investigation. **Joanna Ortyl:** Conceptualization, Methodology, Software, Validation, Investigation, Resources, Data curation, Writing – original draft, Writing – review & editing, Visualization, Supervision, Project administration, Funding acquisition.

## Declaration of competing interest

The authors declare that they have no known competing financial interests or personal relationships that could have appeared to influence the work reported in this paper.

## Acknowledgment

The work was financially supported by the National Centre for Research and Development under the LIDER project (Contract No. LIDER/014/471/L-4/12/NCBR/2013). The authors are also grateful to the National Science Centre - Project SONATA (Contract No. UMO-2012/07/D/ST5/02300) for financing the purchase of steady-state fluorescence spectrofluorometer and to the Foundation for Polish

Science - Project REINTEGRATION (Contract No. POWROTY//2016-1/4) for the equipment for Fluorescence Probe Technique.

## Appendix A. Supplementary data

Supplementary data to this article can be found online at https://doi.org/10.1016/j.porgcoat.2021.106527.

## References


[1] C. Wang, G.O. Brown, D.L. Burris, L.T.J. Korley, T.H. Epps, Coating architects: manipulating multiscale structures to optimize interfacial properties for coating applications, ACS Appl. Polym. Mater. 1 (2019) 2249–2266, https://doi.org/10.1021/acsapm.9b00302.

[2] J. Fang, T. Zhu, J. Sheng, Z. Jiang, Y. Ma, Thickness dependent effective viscosity of a polymer solution near an interface probed by a quartz crystal microbalance with dissipation method, Sci. Rep. 5 (2015) 1–7, https://doi.org/10.1038/srep08491.

[3] X. Gu, L. Shaw, K. Gu, M.F. Toney, Z. Bao, The meniscus-guided deposition of semiconducting polymers, Nat. Commun. 9 (2018) 1–16, https://doi.org/10.1038/s41467-018-02833-9.

[4] K. Heymann, G. Mirschel, T. Scherzer, M.R. Buchmeiser, In-line determination of the thickness of UV-cured coatings on polymer films by NIR spectroscopy, Vib. Spectrosc. 51 (2009) 152–155, https://doi.org/10.1016/j.vibspec.2009.04.001.

[5] D.X. Chen, N. Sun, Z.J. Huang, C.M. Cheng, H. Xu, H.C. Gu, Experimental study on T2 relaxation time of protons in water suspensions of iron-oxide nanoparticles: effects of polymer coating thickness and over-low 1/T2, J. Magn. Magn. Mater. 322 (2010) 548–556, https://doi.org/10.1016/j.jmmm.2009.10.013.

[6] S.C. Lee, N.H. Kwok, H. Guo, W.T. Hung, The effect of wet film thickness on VOC emissions from a finishing varnish, Sci. Total Environ. (2003), https://doi.org/10.1016/S0048-9697(02)00340-6.

[7] A.I. Lavrentyev, S.I. Rokhlin, An ultrasonic method for determination of elastic moduli, density, attenuation and thickness of a polymer coating on a stiff plate, Ultrasonics. 39 (2001) 211–221, https://doi.org/10.1016/S0041-624X(00)00066-4.

[8] P.A. Sørensen, S. Kiil, K. Dam-Johansen, C.E. Weinell, Anticorrosive coatings: a review, J. Coat. Technol. Res. 6 (2009) 135–176, https://doi.org/10.1007/s11998-008-9144-2.

[9] D. Abdeen, M. El Hachach, M. Koc, M. Atieh, A review on the corrosion behaviour of nanocoatings on metallic substrates, Materials. 12 (2019) 210, https://doi.org/10.3390/ma12020210.

[10] M.J. Nine, M.A. Cole, D.N.H. Tran, D. Losic, Graphene: a multipurpose material for protective coatings, J. Mater. Chem. A 3 (2015) 12580–12602, https://doi.org/10.1039/c5ta01010a.

[11] W. Kasprzyk, S. Bednarz, D. Bogdał, G.A. Ameer, T. Świergosz, Cyclodextrin-modified poly(octamethylene citrate) polymers towards enhanced sorption properties, Soft Matter 16 (2020) 3311–3318, https://doi.org/10.1039/c9sm02075f.

[12] S. Luangkularb, S. Prombanpong, V. Tangwarodomnukun, Material consumption and dry film thickness in spray coating process, Procedia CIRP 17 (2014) 789–794, https://doi.org/10.1016/j.procir.2014.02.046.

[13] S. Luangkularb, S. Prombanpong, V. Tangwarodomnukun, Material consumption and dry film thickness in spray coating process, in: Procedia CIRP, Elsevier B.V., 2014, pp. 789–794, https://doi.org/10.1016/j.procir.2014.02.046.

[14] Paint and Coating Testing Manual: 15th. Edition of the Gardner-Sward Handbook, ASTM International, 2012, https://doi.org/10.1520/mnl17-2nd-eb.

[15] R. Talbert, Paint Technology Handbook, CRC Press, 2007, https://doi.org/10.1201/9781420017786.

[16] R. Vatanparast, S. Li, K. Hakala, H. Lemmetyinen, Fluorescenct Probe technology, Macromolecules. 33 (2000) 438–443, https://doi.org/10.1021/ma991414j.

[17] H. Itagaki, K. Horie, I. Mita, Luminescent probe studies of the microstructure and mobility of solid polymers, Prog. Polym. Sci. 15 (1990) 361–424, https://doi.org/10.1016/0079-6700(90)90002-I.

[18] A. Bajorek, K. Trzebiatowska, B. Jędrzejewska, M. Pietrzak, R. Gawinecki, J. Pączkowski, Developing of fluorescence probes based on stilbazolium salts for monitoring free radical polymerization processes. II, J. Fluoresc. 14 (2004) 295–307, https://doi.org/10.1023/B:JOFL.0000024562.60225.d0.

[19] B. Valeur, M.N. Berberan-Santos, Molecular Fluorescence: Principles and Applications, Second edition, Wiley-VCH, Weinheim, Germany, 2012, https://doi.org/10.1002/9783527650002.

[20] J. Ortyl, M. Topa, I. Kamińska-Borek, R. Popielarz, Mechanism of interaction of aminocoumarins with reaction medium during cationic photopolymerization of triethylene glycol divinyl ether, Eur. Polym. J. 116 (2019) 45–55, https://doi.org/10.1016/j.eurpolymj.2019.03.060.

[21] M. Topa, J. Ortyl, A. Chachaj-Brekiesz, I. Kamińska-Borek, M. Pilch, R. Popielarz, Applicability of samarium(III) complexes for the role of luminescent molecular sensors for monitoring progress of photopolymerization processes and control of the thickness of polymer coatings, Spectrochim. Acta A Mol. Biomol. Spectrosc. 199 (2018) 430–440, https://doi.org/10.1016/j.saa.2018.03.050.

[22] J. Ortyl, P. Milart, R. Popielarz, Applicability of aminophthalimide probes for monitoring and acceleration of cationic photopolymerization of epoxides, Polym. Test. 32 (2013) 708–715, https://doi.org/10.1016/j.polymertesting.2013.03.009.

[23] J. Ortyl, R. Popielarz, The performance of 7-hydroxycoumarin-3-carbonitrile and 7-hydroxycoumarin-3-carboxylic acid as fluorescent probes for monitoring of cationic photopolymerization processes by FPT, J. Appl. Polym. Sci. 128 (2013) 1974–1978, https://doi.org/10.1002/app.38378.

[24] M. Topa, F. Petko, M. Galek, J. Ortyl, Double role of diphenylpyridine derivatives as fluorescent sensors for monitoring photopolymerization and the determination of the efficiencies of the generation of superacids by cationic photoinitiators, Sensors (Switz.) 20 (2020), https://doi.org/10.3390/s20113043.

[25] K. Kostrzewska, J. Ortyl, R. Dobosz, J. Kabatc, Squarylium dye and onium salts as highly sensitive photoradical generators for blue light, Polym. Chem. 8 (2017) 3464–3474, https://doi.org/10.1039/c7py00621g.

[26] W. Tomal, D. Krok, A. Chachaj-Brekiesz, J. Ortyl, Beneficial stilbene-based derivatives: from the synthesis of new catalytic photosensitizer to 3D printouts and fiber-reinforced composites, Eur. Polym. J. 156 (2021), 110603, https://doi.org/10.1016/j.eurpolymj.2021.110603.

[27] E. Hola, M. Pilch, J. Ortyl, Thioxanthone derivatives as a new class of organic photocatalysts for photopolymerisation processes and the 3D printing of photocurable resins under visible light, Catalysts. 10 (2020) 1–28, https://doi.org/10.3390/catal10080903.

[28] E. Hola, J. Ortyl, Pyrylium salt as a visible-light-induced photoredox catalyst for polymer and organic synthesis – perspectives on catalyst design and performance, Eur. Polym. J. 150 (2021), 110365, https://doi.org/10.1016/j.eurpolymj.2021.110365.

[29] M.T. Kaczmarek, M. Zabiszak, M. Nowak, R. Jastrzab, Lanthanides: Schiff base complexes, applications in cancer diagnosis, therapy, and antibacterial activity, Coord. Chem. Rev. 370 (2018) 42–54, https://doi.org/10.1016/j.ccr.2018.05.012.

[30] I. Georgieva, T. Mihaylov, N. Trendafilova, Lanthanide and transition metal complexes of bioactive coumarins: molecular modeling and spectroscopic studies, J. Inorg. Biochem. 135 (2014) 100–112, https://doi.org/10.1016/j.jinorgbio.2014.03.003.

[31] V. Balaram, Rare earth elements: a review of applications, occurrence, exploration, analysis, recycling, and environmental impact, Geosci. Front. 10 (2019) 1285–1303, https://doi.org/10.1016/j.gsf.2018.12.005.

[32] J. Garcia, M.J. Allen, Developments in the coordination chemistry of europium(II), Eur. J. Inorg. Chem. (2012) 4550–4563, https://doi.org/10.1002/ejic.201200159.

[33] H. Camargo, T.B. Paolini, E. Niyama, H.F. Brito, M. Cremona, New rare-earth quinolinate complexes for organic light-emitting devices, in: Thin Solid Films, 2013, pp. 36–41, https://doi.org/10.1016/j.tsf.2012.09.085.

[34] M.A. Katkova, M.N. Bochkarev, New trends in design of electroluminescent rare earth metallo-complexes for OLEDs, Dalton Trans. 39 (2010) 6599–6612, https://doi.org/10.1039/c001152e.

[35] H. (Hartmut) Yersin, Highly Efficient OLEDs With Phosphorescent Materials, Wiley-VCH, 2007.

[36] J. Kido, Y. Okamoto, Organo lanthanide metal complexes for electroluminescent materials, Chem. Rev. 102 (2002) 2357–2368, https://doi.org/10.1021/cr010448y.

[37] M.A. Katkova, T.V. Balashova, V.A. Ilichev, A.N. Konev, N.A. Isachenkov, G. K. Fukin, S.Y. Ketkov, M.N. Bochkarev, Synthesis, structures, and electroluminescent properties of scandium N,O-chelated complexes toward near-white organic light-emitting diodes, Inorg. Chem. 49 (2010) 5094–5100, https://doi.org/10.1021/ic1002429.

[38] A. De Bettencourt-Dias, Lanthanide-based emitting materials in light-emitting diodes, J. Chem. Soc., Dalton Trans. (2007) 2229–2241, https://doi.org/10.1039/b702341c.

[39] S.V. Eliseeva, J.C.G. Bünzli, Lanthanide luminescence for functional materials and bio-sciences, Chem. Soc. Rev. 39 (2010) 189–227, https://doi.org/10.1039/b905604c.

[40] Y. Su, D. Zhang, P. Jia, W. Gao, Y. Li, Z. Bai, X. Liu, Q. Deng, J. Xu, C. Yang, Highly selective and sensitive long fluorescence lifetime polyurethane foam sensor based on Tb-complex as chromophore for the detection of H 2 PO 4− in water, Spectrochim. Acta A Mol. Biomol. Spectrosc. 217 (2019) 86–92, https://doi.org/10.1016/j.saa.2019.03.078.

[41] D. Zhang, Y. Zhang, Z. Wang, Y. Zheng, X. Zheng, L. Gao, C. Wang, C. Yang, H. Tang, Y. Li, Biodegradable film enabling visible light excitation of Hexanuclear Europium(III) complex for various applications, J. Lumin. 229 (2021), 117706, https://doi.org/10.1016/j.jlumin.2020.117706.

[42] Y. Su, D. Zhang, P. Jia, W. Gao, Y. Li, J. He, C. Wang, X. Zheng, Q. Yang, C. Yang, Bonded-luminescent foam based on europium complexes as a reversible copper (II) ions sensor in pure water, Eur. Polym. J. 112 (2019) 461–465, https://doi.org/10.1016/j.eurpolymj.2019.01.034.

[43] Y. Lv, Y. Zhao, Z. Yang, C. Liu, H. Yan, G. Li, H. Liu, J. Xie, Luminescent property of a novel rare earth complex Eu(TTA)(2NH2-Phen)3, Synth. Met. 159 (2009) 2530–2533, https://doi.org/10.1016/j.synthmet.2009.09.003.

[44] S. Ćulubrk, Ž. Antić, M. Marinović-Cincović, P.S. Ahrenkiel, M.D. Dramićanin, Synthesis and luminescent properties of rare earth (Sm3+and Eu3+) doped Gd2Ti2O7 pyrochlore nanopowders, Opt. Mater. 37 (2014) 598–606, https://doi.org/10.1016/j.optmat.2014.08.001.

[45] X. Wang, T. Wang, X. Tian, L. Wang, W. Wu, Y. Luo, Q. Zhang, Europium complex doped luminescent solar concentrators with extended absorption range from UV to visible region, Sol. Energy 85 (2011) 2179–2184, https://doi.org/10.1016/j.solener.2011.06.007.

[46] H.Q. Chen, J. Fu, L. Wang, B. Ling, B. Bin Qian, J.G. Chen, C.L. Zhou, Ultrasensitive mercury(II) ion detection by europium(III)-doped cadmium sulfide composite nanoparticles, Talanta. 83 (2010) 139–144, https://doi.org/10.1016/j.talanta.2010.08.052.

[47] A. Duerkop, M. Turel, A. Lobnik, O.S. Wolfbeis, Microtiter plate assay for phosphate using a europium-tetracycline complex as a sensitive luminescent probe, Anal. Chim. Acta 555 (2006) 292–298, https://doi.org/10.1016/j.aca.2005.09.007.
[48] W.G. Quirino, R.D. Adati, S.A.M. Lima, C. Legnani, M. Jafelicci, M.R. Davolos, M. Cremona, Electroluminescence of a device based on europium β-diketonate with phosphine oxide complex, Thin Solid Films 515 (2006) 927–931, https://doi.org/10.1016/j.tsf.2006.07.066.
[49] M. Bala, S. Kumar, P. Boora, V.B. Taxak, A. Khatkar, S.P. Khatkar, Enhanced optoelectronics properties of europium(III) complexes with β-diketone and nitrogen heterocyclic ligands, J. Mater. Sci. Mater. Electron. 25 (2014) 2850–2856, https://doi.org/10.1007/s10854-014-1951-x.
[50] D. Wang, Y. Pi, C. Zheng, L. Fan, Y. Hu, X. Wei, Preparation and photoluminescence of some europium (III) ternary complexes with β-diketone and nitrogen heterocyclic ligands, J. Alloys Compd. 574 (2013) 54–58, https://doi.org/10.1016/j.jallcom.2013.04.049.
[51] R. Reyes, M. Cremona, E.E.S. Teotonio, H.F. Brito, O.L. Malta, Electrophosphorescence emission in organic light-emitting diodes based on (Sm+Eu) complexes, Thin Solid Films 469–470 (2004) 59–64, https://doi.org/10.1016/j.tsf.2004.06.184.
[52] Y. Su, J. Yu, Y. Li, S.F.Z. Phua, G. Liu, W.Q. Lim, X. Yang, R. Ganguly, C. Dang, C. Yang, Y. Zhao, Versatile bimetallic lanthanide metal-organic frameworks for tunable emission and efficient fluorescence sensing, Commun. Chem. 1 (2018), https://doi.org/10.1038/s42004-018-0016-0.
[53] P. Jia, Z. Wang, Y. Zhang, D. Zhang, W. Gao, Y. Su, Y. Li, C. Yang, Selective sensing of Fe3+ ions in aqueous solution by a biodegradable platform based lanthanide metal organic framework, Spectrochim. Acta A Mol. Biomol. Spectrosc. 230 (2020), 118084, https://doi.org/10.1016/j.saa.2020.118084.
[54] C. Yang, S. Liu, J. Xu, Y. Li, M. Shang, L. Lei, G. Wang, J. He, X. Wang, M. Lu, Efficient red emission from poly(vinyl butyral) films doped with a novel europium complex based on a terpyridyl ancillary ligand: synthesis, structural elucidation by Sparkle/RM1 calculation, and photophysical properties, Polym. Chem. 7 (2016) 1147–1157, https://doi.org/10.1039/c5py01956g.
[55] G. Marriott, M. Heidecker, E.P. Diamandis, Y. Yan-Marriott, Time-resolved delayed luminescence image microscopy using an europium ion chelate complex, Biophys. J. 67 (1994) 957–965, https://doi.org/10.1016/S0006-3495(94)80597-1.
[56] J.C.G. Bünzli, Lanthanide luminescent bioprobes (LLBs), Chem. Lett. 38 (2009) 104–109, https://doi.org/10.1246/cl.2009.104.
[57] N. Gahlaut, L.W. Miller, Time-resolved microscopy for imaging lanthanide luminescence in living cells, Cytometry A 77 A (2010) 1113–1125, https://doi.org/10.1002/cyto.a.20964.
[58] M. Lin, Y. Zhao, S.Q. Wang, M. Liu, Z.F. Duan, Y.M. Chen, F. Li, F. Xu, T.J. Lu, Recent advances in synthesis and surface modification of lanthanide-doped upconversion nanoparticles for biomedical applications, Biotechnol. Adv. 30 (2012) 1551–1561, https://doi.org/10.1016/j.biotechadv.2012.04.009.
[59] S. Gai, P. Yang, C. Li, W. Wang, Y. Dai, N. Niu, J. Lin, Synthesis of magnetic, up-conversion luminescent, and mesoporous core-shell-structured nanocomposites as drug carriers, Adv. Funct. Mater. 20 (2010) 1166–1172, https://doi.org/10.1002/adfm.200902274.
[60] D.B. Craig, Z. Hiebert, Analysis of complexes of metabolites with europium tetracycline using capillary electrophoresis coupled with laser-induced luminescence detection, BioMetals. 30 (2017) 449–458, https://doi.org/10.1007/s10534-017-0018-x.
[61] S. Zhang, P. Winter, K. Wu, A.D. Sherry, A novel europium(III)-based MRI contrast agent [10], J. Am. Chem. Soc. 123 (2001) 1517–1518, https://doi.org/10.1021/ja005820q.
[62] Y. Wu, T.C. Soesbe, G.E. Kiefer, P. Zhao, A.D. Sherry, A responsive europium(III) chelate that provides a direct readout of pH by MRI, J. Am. Chem. Soc. 132 (2010) 14002–14003, https://doi.org/10.1021/ja106018n.
[63] N.O. Nuñez, M. García, J. García-Sevillano, S. Rivera-Fernández, J.M. De La Fuente, M. Ocaña, One-step synthesis and polyacrylic acid functionalization of multifunctional europium-doped NaGdF4 nanoparticles with selected size for optical and MRI imaging, Eur. J. Inorg. Chem. 2014 (2014) 6075–6084, https://doi.org/10.1002/ejic.201402690.
[64] M. Starck, P. Kadjane, E. Bois, B. Darbouret, A. Incamps, R. Ziessel, L. J. Charbonnière, Towards libraries of luminescent lanthanide complexes and labels from generic synthons, Chem. Eur. J. 17 (2011) 9164–9179, https://doi.org/10.1002/chem.201100390.
[65] D.F. Eaton, Reference materials for fluorescence measurement, Pure Appl. Chem. 60 (1988) 1107–1114, https://doi.org/10.1351/pac198860071107.
[66] D. Nowak, J. Ortyl, I. Kamińska-Borek, K. Kukuła, M. Topa, R. Popielarz, Photopolymerization of hybrid monomers: part I: comparison of the performance of selected photoinitiators in cationic and free-radical polymerization of hybrid monomers, Polym. Test. 64 (2017) 313–320, https://doi.org/10.1016/j.polymertesting.2017.10.020.
[67] Shyama P. Sinha, Complexes of the Rare Earths - 1st Edition. https://www.elsevier.com/books/complexes-of-the-rare-earths/sinha/978-0-08-011616-7, 1966. (Accessed 4 May 2021).